

A GLOBALLY CONVERGENT FLOW FOR TIME-DEPENDENT MEAN FIELD GAMES AND A SOLVER-AGNOSTIC FRAMEWORK FOR INVERSE PROBLEMS

HANWEI YAN¹, XIANJIN YANG^{2,*}, JINGGUO ZHANG³

¹*Department of Mathematics, City University of Hong Kong, Hong Kong, China.*

²*Department of Computing and Mathematical Sciences, California Institute of Technology, CA, USA.*

³*Department of Mathematics and Risk Management Institute, National University of Singapore, Singapore.*

ABSTRACT. Mean field games (MFGs) model the limit of large populations of strategically interacting agents, yet both forward and inverse problems remain challenging. For the forward problem, a difficulty is to design numerical methods with global convergence guarantees whose convergence does not depend on careful initialization. For the inverse problem, a difficulty is to decouple parameter optimization from the forward solver, so that parameter updates do not depend on implementation details, and the inverse method does not need to be reformulated when the forward solver is changed. We address both issues as follows. For the forward problem, we propose a monotone Hessian–Riemannian flow for time-dependent MFGs on the feasible manifold of densities. The flow preserves the positivity of densities and is proved to be globally convergent. For the inverse problem, we cast parameter estimation as an outer optimization problem over the unknown coefficients, with the MFG system solved in an inner step for each parameter value. For solving this problem, we consider an adjoint-based gradient method together with a Gauss–Newton acceleration. This leads to a solver-agnostic framework, in which parameter updates are computed by implicitly differentiating the discrete MFG equations satisfied by the converged MFG solution, rather than by differentiating through a particular forward solver. We demonstrate the approach on several stationary and time-dependent MFG examples, where the Gauss–Newton method consistently requires fewer outer iterations than gradient descent.

Keywords: mean field games, monotone flows, inverse problems, solver-agnostic, Gauss–Newton method

1. INTRODUCTION

In this paper, we develop a globally convergent method for time-dependent mean field games (MFGs) whose convergence does not rely on careful initialization, together with a solver-agnostic framework for inverse MFG problems in which parameter optimization is decoupled from the numerical procedure used to solve the forward problem. MFGs describe the macroscopic limit of strategic interactions among a large population of indistinguishable agents. MFGs are introduced independently by two research groups: one led by Lasry and Lions [38–40], and the other by Caines, Huang, and Malhamé [31, 32]. The theory offers a powerful mathematical framework for approximating Nash equilibria in multi-agent systems with a finite number of players. Under the assumptions of a homogeneous population and symmetric interactions, the MFG model demonstrates that as the number of agents approaches infinity, the influence of any specific opponent vanishes: the strategy of an individual agent is shaped by the aggregate behavior of the population, which is statistically represented by the mean field. This viewpoint is particularly natural in large financial markets, where each small trader has a negligible individual impact on prices, yet the aggregate trading behavior of the population can significantly affect market dynamics [16, 37]. In finite N -player games, the computational complexity of finding a Nash equilibrium grows exponentially with N . The solution obtained from the MFG framework is an ε -Nash equilibrium, which provides an effective approximation to the Nash equilibrium in such finite-player settings. A standard MFG system is characterized by a Hamilton–Jacobi–Bellman (HJB) equation coupled

E-mail address: hanweiyang2-c@my.cityu.edu.hk, yxjmath@caltech.edu, e0983423@u.nus.edu.

*Corresponding author. Authors are listed in alphabetical order.

with a Fokker–Planck (FP) equation. The former governs the value function of a representative agent, while the latter describes the evolution of the population distribution.

A prototypical time-dependent MFG on the d -dimensional torus \mathbb{T}^d takes the form

$$\begin{cases} -\partial_t u - \nu \Delta u + H(x, D_x u) = f(m) + V(x), & \forall x \in \mathbb{T}^d \times (0, T), \\ m_t - \nu \Delta m - \operatorname{div}(D_p H(x, D_x u) m) = 0, & \forall x \in \mathbb{T}^d \times (0, T), \\ m(x, 0) = m_0(x), \quad u(x, T) = u_T(x), & \forall x \in \mathbb{T}^d, \end{cases} \quad (1.1)$$

where u denote the value function for an agent, m represent the probability density function, ν is a volatility parameter of agent's movement. We use H to represent the Hamiltonian, f stands for the coupling term, and V is the spatial cost. The initial distribution and the terminal cost are denoted by m_0 and u_T . In the MFG system (1.1), the optimal strategy for a representative agent is given by $-D_p H(x, D_x u)$ [38–40]. In this paper, we also consider the stationary MFG, which takes the form of

$$\begin{cases} -\nu \Delta u + H(x, D_x u) = f(m) + V(x) + \lambda, & \forall x \in \mathbb{T}^d, \\ -\nu \Delta m - \operatorname{div}(D_p H(x, D_x u) m) = 0, & \forall x \in \mathbb{T}^d, \\ \int_{\mathbb{T}^d} u \, dx = 0, \quad \int_{\mathbb{T}^d} m \, dx = 1. \end{cases} \quad (1.2)$$

The stationary MFG system can be interpreted as the long-time limit $t \rightarrow \infty$ of the time-dependent MFG [14, 15].

MFG has been widely applied in engineering, economics, finance, and energy distribution networks. For comprehensive overviews, see [17, 25]. As a highly coupled system, MFG rarely admits closed-form solutions, which motivates the development of efficient numerical methods for their approximation.

Solving either the stationary MFG (1.2) or the time-dependent MFG (1.1) can be formulated as finding zeros of nonlinear operators acting on infinite-dimensional function spaces. In the stationary case, the ergodic constant λ can be eliminated explicitly, yielding a closed operator equation in (m, u) alone. Indeed, multiplying the Hamilton–Jacobi equation by m and integrating over \mathbb{T}^d , using periodicity, gives

$$\lambda(m, u) = \frac{\int_{\mathbb{T}^d} \left(-\nu \Delta u + H(x, D_x u) - f(m(x)) - V(x) \right) m(x) \, dx}{\int_{\mathbb{T}^d} m \, dx}. \quad (1.3)$$

With (1.3) in hand, define the stationary residual operator

$$\mathcal{F}_{\text{st}} \begin{pmatrix} m \\ u \end{pmatrix} := \begin{pmatrix} \nu \Delta u - H(x, D_x u) + f(m) + V(x) + \lambda(m, u) \\ -\nu \Delta m - \operatorname{div}(D_p H(x, D_x u) m) \end{pmatrix}, \quad x \in \mathbb{T}^d. \quad (1.4)$$

Then, solving the stationary MFG (1.2) is equivalent to finding (m, u) such that

$$\mathcal{F}_{\text{st}}(m, u) = 0, \quad \int_{\mathbb{T}^d} m(x) \, dx = 1, \quad m(x) \geq 0, \quad \int_{\mathbb{T}^d} u(x) \, dx = 0.$$

For the time-dependent problem, one analogously introduces the evolution residual operator

$$\mathcal{F}_{\text{td}} \begin{pmatrix} m \\ u \end{pmatrix} := \begin{pmatrix} \mathcal{F}_{\text{td}}^{\text{HJB}}(m, u) \\ \mathcal{F}_{\text{td}}^{\text{FP}}(m, u) \end{pmatrix} := \begin{pmatrix} \partial_t u + \nu \Delta u - H(x, D_x u) + f(m) + V(x) \\ \partial_t m - \nu \Delta m - \operatorname{div}(D_p H(x, D_x u) m) \end{pmatrix}, \quad (t, x) \in (0, T) \times \mathbb{T}^d, \quad (1.5)$$

so that solving (1.1) amounts to finding (m, u) satisfying $\mathcal{F}_{\text{td}}(m, u) = 0$ together with the prescribed initial-terminal data and the constraints $m(t, \cdot) \geq 0$ and $\int_{\mathbb{T}^d} m(t, x) \, dx = 1$ for all $t \in [0, T]$.

From this operator viewpoint, one may apply Newton-type iterations to a finite-difference discretization of the coupled residual equations together with the normalization constraints [2]. While highly effective when initialized sufficiently close to a solution, such Newton solvers are well known to exhibit primarily local convergence. A possible way to obtain a globally convergent algorithm is to recast the MFG system as the first-order optimality condition of a linearly constrained convex minimization problem. This structure corresponds to so-called potential MFGs, for which one can leverage convex optimization methods (see, e.g., [9–11]). This approach, however, is limited to potential MFGs and does not extend to MFGs with a non-potential structure, such as (4.4) in Section 4.2.2. A different direction relaxes the potential assumption and instead exploits that the MFG residual operators \mathcal{F}_{st} and \mathcal{F}_{td} are monotone under the Lasry–Lions

monotonicity condition [5, 38, 39]. To illustrate the idea, let $z = (m, u)$ and let \mathcal{F} denote either \mathcal{F}_{st} or \mathcal{F}_{td} , viewed as a mapping between suitable Hilbert spaces. We equip the product space with the pairing,

$$\langle z_1, z_2 \rangle := \int_{\mathbb{T}^d} \int_{\mathbb{T}^d} m_1(x)m_2(x) dx + u_1(x)u_2(x) dx, \quad \|z\|^2 := \langle z, z \rangle,$$

and analogously in the time-dependent setting by integrating over $(0, T) \times \mathbb{T}^d$. Monotonicity then means that

$$\langle \mathcal{F}(z_1) - \mathcal{F}(z_2), z_1 - z_2 \rangle \geq 0 \quad \text{for all admissible } z_1, z_2.$$

This property naturally suggests introducing an artificial-time evolution (a monotone flow)

$$\partial_s z(s) = -\mathcal{F}(z(s)), \quad s \geq 0, \tag{1.6}$$

for which one formally obtains the dissipation estimate

$$\frac{d}{ds} \frac{1}{2} \|z(s) - z^*\|^2 = -\langle \mathcal{F}(z(s)) - \mathcal{F}(z^*), z(s) - z^* \rangle \leq 0$$

whenever z^* satisfies $\mathcal{F}(z^*) = 0$. Therefore, provided the initial guess is admissible, the resulting flow is globally well defined for all artificial times $s \geq 0$. Furthermore, if the Hamiltonian H is strongly convex (in the momentum variable) and the coupling f is strongly monotone in the standard Lasry–Lions sense, then the monotone flow is globally convergent: for any admissible initial datum, the trajectory exists for all $s \geq 0$ and converges as $s \rightarrow \infty$ to the unique solution of the MFG system [5].

The key obstruction is that (1.6) is an ambient flow: it evolves in the full product space and does not enforce the intrinsic constraints of the MFG system, in particular $m \geq 0$ and mass conservation. As a result, positivity of the density is not preserved in general. This issue is especially severe computationally: once an iterate leaves the positive cone, nonlinearities such as $f(m)$ can become numerically unstable (e.g., for entropic couplings $f(m) = \ln m$).

To enforce positivity of densities in stationary MFGs, [28] introduced a monotone flow on the manifold of probability densities equipped with a barrier-induced Riemannian geometry, leading to Hessian–Riemannian flows (HRFs) that preserve positivity by construction. The idea is to work on the open set of strictly positive densities and equip (m, u) with the Riemannian metric generated by the entropy functional

$$\int_{\mathbb{T}^d} \left(m \ln m - m + \frac{1}{2} u^2 \right) dx.$$

The corresponding Hessian induces the weighted pairing

$$\langle (\delta m, \delta u), (\delta \tilde{m}, \delta \tilde{u}) \rangle = \int_{\mathbb{T}^d} \frac{\delta m \delta \tilde{m}}{m} dx + \int_{\mathbb{T}^d} \delta u \delta \tilde{u} dx.$$

The ambient monotone flow direction, $-\mathcal{F}_{\text{st}}$, is then projected onto the manifold of positive densities with respect to this Riemannian metric, yielding an intrinsic monotone flow. This yields the positivity-preserving HRF [28]

$$\begin{pmatrix} \partial_s m \\ \partial_s u \end{pmatrix} = - \begin{pmatrix} m & 0 \\ 0 & 1 \end{pmatrix} \mathcal{F}_{\text{st}} \begin{pmatrix} m \\ u \end{pmatrix}.$$

This multiplicative structure is the key point: one can rewrite the first equation as an evolution for $\ln m$, so strict positivity of the initial density propagates for all artificial times $s \geq 0$, while $\int_{\mathbb{T}^d} m dx$ is preserved by construction; see, e.g., [28].

However, extending the HRF method to the time-dependent PDE system (1.1) involves additional constraints: one must simultaneously preserve positivity at each time slice and enforce the mixed initial-terminal conditions $m(x, 0) = m_0(x)$ and $u(x, T) = u_T(x)$. A constrained-flow viewpoint proposed in [26] suggests treating these endpoint conditions as trace constraints at $t = 0$ and $t = T$. This naturally leads to a time-regularity setting in which traces are well defined, typically a Sobolev space with one time derivative, together with a projection operator that enforces the two endpoint constraints simultaneously. Such a projection is inherently global in time: for a given direction, computing its projection onto the feasible manifold amounts to solving an auxiliary two-point boundary-value problem in the time variable. The same difficulty reappears when one attempts to introduce a Riemannian geometry in order to guarantee positivity at the continuous level. We refer to Section 2 for further discussion.

The difficulty described above stems from the trace-regularity requirements and the global-in-time projection inherent in continuous-in-time approaches. This naturally motivates a fully discrete viewpoint: once the system is discretized in time, the mixed endpoint conditions become coordinate constraints on the first and last time-slices, and positivity and mass conservation reduce to algebraic conditions on finite-dimensional vectors. Both difficulties thus disappear. Feasibility can be maintained simply by freezing the boundary slices and evolving only the interior degrees of freedom, reducing constraint handling to an explicit elimination of boundary variables. Following this discretize-then-flow strategy, we construct an HRF directly for the time-discretized MFG system. The resulting artificial-time dynamics evolve intrinsically on the admissible set while preserving positivity and mass conservation of the density, and are proved to be globally convergent. All details are deferred to Section 2.

Under standard assumptions, such as convexity of the Hamiltonian H and Lasry–Lions monotonicity of the coupling f , we prove that the proposed HRF for the time-discretized MFG is globally convergent to the unique solution of the discretized version of (1.1); see Theorem 2.4. Moreover, the density component remains strictly positive along the entire flow; see Proposition 2.3.

The second contribution concerns inverse problems for both stationary and time-dependent MFGs. We develop algorithms for MFG inverse problems, in which unknown model components (such as the density of agents, the value function, or the spatial cost) are inferred from partial, noisy observations of the population and the spatial cost. Such problems arise, for example, in financial markets, where one seeks to recover latent trading costs or risk premia from order-flow and price data generated by a large population of interacting agents, and in models of crowd motion, where spatial preferences are inferred from observed mass evolution. More concretely, in the settings of (1.2) and (1.1), one seeks to recover the solution (m, u) (possibly λ for (1.2)), given noisy observations of the spatial cost V and m at some observations points and we assume that we know H and f and ν . A concrete description of the inverse problem can be seen in Problem 1 and Problem 2 of Section 3. We formulate the inverse problem as a nonlinear optimization problem constrained by the MFG equations, with the spatial cost V as the parameter to be optimized. The objective balances data fidelity and the regularity of the unknowns. The constraint is that (m, u) must satisfy the (stationary or time-dependent) MFG system for the current V .

This formulation differs from several recent approaches to inverse problems for MFGs that treat the unknown coefficients and the MFG state as joint decision variables in a single optimization problem, and minimize over both simultaneously, see [23, 47]. In contrast, our viewpoint is closer in spirit to bilevel formulations [30, 51, 60, 61], where the outer problem updates only the coefficients, while the inner problem computes the corresponding MFG state by solving the forward system. The bilevel formulation offers two practical advantages. First, for each parameter value, the forward step returns the corresponding MFG solution, so the outer objective is always evaluated at a state that satisfies the MFG equations. Second, it decouples the outer optimization from the particular algorithm used for the inner MFG solve. As a result, one can change the inner solver, stopping criteria, or implementation details without modifying the outer optimization procedure, provided the forward solve is sufficiently accurate. However, most existing bilevel approaches compute outer gradients in a way that is tightly coupled to the chosen inner procedure, either by differentiating through a particular solver and its iteration trace [60, 61], or by committing to a specific linearization such as policy iteration [51, 58, 59]. Instead, we adopt a solver-agnostic approach inspired by implicit differentiation [4, 6, 8]: we treat the converged discrete MFG system as an implicit hidden layer and differentiate the constraints at the solution rather than through the solver iterations. The forward solver thus only needs to return a sufficiently accurate solution, and can be changed without modifying the outer optimization procedure. Building on this, our second contribution is a solver-agnostic framework for inverse problems in both stationary and time-dependent MFGs, supporting both adjoint-based first-order updates and Gauss–Newton (GN) acceleration for the outer optimization. Further details are deferred to Section 3.

Overall, our contributions can be summarized as follows:

1. *A globally convergent, positivity-preserving flow method for time-dependent MFGs.* We follow a discretize-then-flow strategy. After space-time discretization, we enforce the mixed endpoint conditions by freezing the boundary slices and evolving only the interior unknowns. On the resulting finite-dimensional system, we construct an HRF that preserves positivity of the density. The global convergence of the HRF to the solution of the discretized MFG system is guaranteed.

2. *Plug-and-play, solver-agnostic methods for inverse problems in stationary and time-dependent MFGs.*

We pose the inverse problem as a nonlinear optimization problem constrained by the MFG equations, with unknown coefficients such as the spatial cost as decision variables. The framework is plug-and-play: any forward solver that returns a sufficiently accurate solution of the MFG can be used. Within this framework, we consider both a first-order method and a GN acceleration for the inverse problems.

1.1. Related Work on Numerical Methods and Inverse Problems for MFGs. In recent years, a broad range of numerical methods has been developed for forward MFG problems. For the purposes of the present discussion, it is convenient to group them loosely into direct discretization methods, optimization-based methods, and learning-based methods.

Direct discretization methods work directly with a spatial or space-time discretization of the MFG system and solve the resulting finite-dimensional equations. Representative examples include finite difference schemes [1–3], semi-Lagrangian and Lagrange–Galerkin discretizations [18, 19], and finite element approximations [49], together with iterative solvers such as Newton-type methods, policy iteration [3, 12, 41], and monotone flows [5, 28].

A second class consists of optimization-based methods, which exploit additional structure in the MFG system before solving it numerically. For potential MFGs, primal-dual algorithms reformulate the problem as a variational problem [9, 10]. Related Fourier-based approaches for nonlocal couplings also fall into this category, where nonlocal terms are represented in a reduced form that supports variational, splitting, or primal-dual algorithms [44, 45, 48].

A third class comprises learning-based methods. Neural-network-based solvers offer flexible function approximations for MFG systems [20, 21, 42, 53], and Gaussian process (GP) methods, originally developed as Bayesian nonparametric surrogates for PDEs [22, 56, 57], have also been adapted to MFGs [46, 47, 58]. While these approaches have shown promising empirical performance, global convergence guarantees remain less well understood for this class of methods.

For the purposes of this paper, the most relevant solver family is that of monotonicity-based flow methods for directly discretized MFG systems. Under the Lasry–Lions monotonicity condition, the MFG system can be viewed as a root-finding problem for a monotone operator, which motivates flow-based solvers. Monotone flow schemes for stationary MFGs appear in [5], and related monotone schemes in the finite-state setting are introduced in [26]. The flow viewpoint is further extended to time-dependent MFGs in the finite-state case in [27]. A key advantage of this line of work is that it provides a mechanism for global convergence without requiring the MFG system to admit a potential structure. To preserve positivity of the density, [28] introduced an HRF methodology for stationary MFGs, which preserves both positivity and mass by incorporating a geometry adapted to the density constraint. More recently, [7] extended the HRF approach to multi-population Wardrop equilibrium problems on generalized graphs. However, for time-dependent MFGs, extending HRF is substantially more delicate because one must simultaneously handle positivity, mass conservation, and mixed initial-terminal conditions. Our first contribution is aimed precisely at this gap.

Inverse problems for MFGs aim to reconstruct unknown coefficients, such as spatial costs or coupling functions, from partial and possibly noisy observations [23, 43]. On the theoretical side, these problems have also been studied through convexification and related stability analyses [33, 35, 36, 52]. In this paper, our focus is on numerical methodologies.

From a numerical viewpoint, one class of approaches adopts an all-at-once formulation, in which the unknown coefficients and the MFG state are optimized simultaneously [23, 29, 58]. A second class adopts a bilevel viewpoint, in which the outer problem updates the unknown coefficients while the inner problem solves the MFG system for the current parameter value [30, 51, 60, 61]. Distinct from these optimization-based formulations, a related recent direction is provided by learning-based methods, such as [55], which use operator-learning ideas to leverage information across multiple MFG instances rather than solving each inverse problem independently.

A common feature of many existing bilevel pipelines is that the outer gradient is constructed together with a particular inner solver, so that its computation may depend on solver-specific implementation details such as the iterative scheme, the number of inner iterations, and the stopping criterion. This motivates the solver-agnostic framework developed in this paper, in which the outer optimization is carried out over the unknown coefficients while the gradient is obtained by implicitly differentiating the discrete MFG system satisfied by

the converged inner solution, rather than by differentiating through the iteration trace of a particular forward solver. We note that [61] also uses an adjoint-based strategy to obtain a solver-agnostic framework. The key distinction lies in the level at which implicit differentiation is performed. In [61], which focuses on potential MFGs, the adjoint is derived from the optimality system of an inner PDE-constrained convex minimization problem. By contrast, we differentiate the discrete MFG system satisfied by the converged inner solution directly, which does not require the MFG to admit a potential or variational structure.

1.2. Outlines. The remainder of this paper is organized as follows. Section 2 develops the HRF method for time-dependent MFGs. Section 3 presents a solver-agnostic framework for inverse problems. Numerical experiments are reported in Section 4. Section 5 concludes the paper and outlines directions for future research. Finally, all proofs are collected in Appendix A. To streamline the exposition, we do not restate this convention in the main text.

2. HRFs FOR TIME-DEPENDENT MFGs

The goal of this section is to develop a flow-based solver for (1.1) that preserves the positivity of the density and admits global convergence guarantees driven by monotonicity. To focus on the main ideas without being distracted by the treatment of boundary conditions and low-regularity solutions, we work in the setting of classical solutions. Throughout, we assume that (1.1) admits a unique classical solution (m, u) , where $m, u \in C^{2,1}(\mathbb{T}^d \times [0, T])$. Classical well-posedness holds under standard hypotheses; see [13, 24, 39] for the time-dependent MFG system and detailed proofs. In the continuous setting, we rely on standard conditions ensuring well-posedness and regularity, such as the convexity of H in the momentum variable and the Lasry–Lions monotonicity of the coupling f . Since our HRF construction is carried out at the fully discrete level, we do not restate the corresponding continuous hypotheses here and instead state explicitly the discrete assumptions needed to guarantee convergence of the discrete MFG solver.

The HRF method of [28] is developed for stationary MFGs and shown to be globally convergent. In what follows, we first outline the main obstacles to extending this approach to time-dependent MFGs at the continuous level. Guided by these observations, we then develop an HRF method for time-dependent MFGs from a fully discrete perspective.

2.1. Challenges in Constructing the HRF for Time-Dependent MFGs. In this subsection, we explore how one might extend the HRF of [28] to time-dependent MFGs at the continuous PDE level, and identify the resulting challenges.

We define

$$\mathcal{X} := \left\{ (m, u) : m \in C^{2,1}(\mathbb{T}^d \times [0, T]), u \in C^{2,1}(\mathbb{T}^d \times [0, T]) \right\},$$

together with the residual space

$$\mathcal{Y} := C(\mathbb{T}^d \times [0, T]) \times C(\mathbb{T}^d \times [0, T]).$$

We recall the time-dependent MFG residual operator $\mathcal{F}_{\text{td}} : \mathcal{X} \rightarrow \mathcal{Y}$ defined in (1.5). Denote $z := (m, u)$. Solving (1.1) is equivalent to finding $z \in \mathcal{X}$ such that $\mathcal{F}_{\text{td}}(z) = 0$, subject to the endpoint conditions. Define

$$C : \mathcal{X} \rightarrow \mathcal{E}, \quad C(m, u) := (m(\cdot, 0) - m_0, u(\cdot, T) - u_T), \quad \mathcal{E} := C(\mathbb{T}^d) \times C(\mathbb{T}^d). \quad (2.1)$$

The endpoint-feasible set is the affine manifold

$$\mathcal{M} := \{z \in \mathcal{X} : Cz = 0\},$$

with tangent space at any $z \in \mathcal{M}$ given by

$$T_z \mathcal{M} = \ker C = \left\{ (\delta m, \delta u) \in \mathcal{X} : \delta m(\cdot, 0) = 0, \delta u(\cdot, T) = 0 \right\}.$$

To enforce positivity of the density along the flow, we restrict attention to

$$\mathcal{M}_{++} := \{(m, u) \in \mathcal{M} : m(x, t) > 0 \text{ for all } (x, t) \in \mathbb{T}^d \times [0, T]\}.$$

On \mathcal{M}_{++} , we equip the density component with an entropy-type metric and keep the Euclidean metric in u . For $z = (m, u) \in \mathcal{M}_{++}$ we define the weighted inner product

$$\langle (\delta m, \delta u), (\delta \tilde{m}, \delta \tilde{u}) \rangle_{\mathcal{H}(z)} := \int_0^T \int_{\mathbb{T}^d} \frac{\delta m \delta \tilde{m}}{m} dx dt + \int_0^T \int_{\mathbb{T}^d} \delta u \delta \tilde{u} dx dt,$$

corresponding to the diagonal metric operator

$$\mathcal{H}(z) = \text{diag}(1/m, I), \quad \mathcal{H}(z)^{-1} = \text{diag}(m, I).$$

The weight $1/m$ penalizes variations increasingly as $m \rightarrow 0$, providing the barrier mechanism that keeps the density away from the boundary of the nonnegative cone. A natural extension of the HRF idea of [28] is then to evolve z in artificial time along the direction $-\mathcal{H}(z)^{-1}\mathcal{F}_{\text{td}}(z)$, giving the flow

$$\begin{pmatrix} \partial_s m \\ \partial_s u \end{pmatrix} = -\mathcal{H}(z)^{-1}\mathcal{F}_{\text{td}}(z) = -\begin{pmatrix} m \mathcal{F}_{\text{td}}^m(m, u) \\ \mathcal{F}_{\text{td}}^u(m, u) \end{pmatrix}, \quad (2.2)$$

where we write $\mathcal{F}_{\text{td}}(z) = (\mathcal{F}_{\text{td}}^m(m, u), \mathcal{F}_{\text{td}}^u(m, u))$. In particular, the density component satisfies

$$\partial_s m(x, t) = -m(x, t) \mathcal{F}_{\text{td}}^m(m, u)(x, t),$$

so the instantaneous velocity vanishes wherever $m = 0$, which keeps m positive. However, the flow (2.2) does not, in general, preserve the endpoint conditions: even if $z(0) \in \mathcal{M}$, one typically has $z(s) \notin \mathcal{M}$ for $s > 0$. A remedy for preserving endpoint conditions along monotone flows, formulated independently of any Riemannian geometry, is proposed in [26]. The basic mechanism is to project the driving field onto the tangent space $T_z\mathcal{M} = \ker C$, so that feasibility is maintained along the flow. To make endpoint evaluation continuous and the projection well-posed in a Hilbert setting, one works in the space

$$\mathcal{X}_{H^1} := H^1(0, T; L^2(\mathbb{T}^d)) \times H^1(0, T; L^2(\mathbb{T}^d)),$$

equipped with the inner product

$$\langle (\delta m, \delta u), (\delta \tilde{m}, \delta \tilde{u}) \rangle_{H^1} := \int_0^T \int_{\mathbb{T}^d} (\delta m \delta \tilde{m} + \partial_t \delta m \partial_t \delta \tilde{m}) \, dx \, dt + \int_0^T \int_{\mathbb{T}^d} (\delta u \delta \tilde{u} + \partial_t \delta u \partial_t \delta \tilde{u}) \, dx \, dt.$$

Given an ambient direction $w \in \mathcal{X}_{H^1}$, its H^1 -orthogonal projection onto $\ker C$ is the unique minimizer of

$$\Pi_{\perp} w \in \arg \min_{v \in \mathcal{X}_{H^1}} \left\{ \frac{1}{2} \|v\|_{H^1}^2 - \langle v, w \rangle_{L^2} \right\} \quad \text{subject to} \quad Cv = 0, \quad (2.3)$$

where $\langle \cdot, \cdot \rangle_{L^2}$ denotes the standard space-time pairing. The optimality conditions for (2.3) show that, even though the constraint only fixes endpoint values, the correction generated by the H^1 projection is spread across the full interval $(0, T)$, and computing $\Pi_{\perp} w$ requires solving two-point boundary value problems in t for each spatial degree of freedom.

If one further wishes to incorporate the Riemannian geometry in order to also guarantee positivity of the density, the two requirements must be combined. One natural approach is to work in \mathcal{X}_{H^1} and endow it, at each $z = (m, u) \in \mathcal{M}_{++}$, with the z -dependent inner product

$$\langle (\delta m, \delta u), (\delta \tilde{m}, \delta \tilde{u}) \rangle_{H^1, z} := \int_0^T \int_{\mathbb{T}^d} \frac{\delta m \delta \tilde{m} + \partial_t \delta m \partial_t \delta \tilde{m}}{m} \, dx \, dt + \int_0^T \int_{\mathbb{T}^d} (\delta u \delta \tilde{u} + \partial_t \delta u \partial_t \delta \tilde{u}) \, dx \, dt, \quad (2.4)$$

which is trace compatible in time and incorporates the positivity barrier in the density component. The constrained update direction $v(z)$ is then defined by

$$v(z) \in \arg \min_{v \in \mathcal{X}_{H^1}} \left\{ \frac{1}{2} \|v\|_{H^1, z}^2 + \langle \mathcal{F}_{\text{td}}(z), v \rangle_{L^2} \right\} \quad \text{subject to} \quad Cv = 0, \quad (2.5)$$

with the artificial-time update given by $\partial_s z = v(z)$. While this formulation simultaneously enforces endpoint feasibility and positivity, its computational cost is even higher: the optimality conditions for (2.5) require solving a subproblem that is second order in time with state-dependent coefficients through (2.4), making each artificial-time step considerably more expensive.

The difficulty in both cases above stems from the continuous setting: enforcing endpoint conditions requires working in a trace-compatible function space, and the resulting projection is inherently global in time. In a fully discrete setting, this difficulty disappears entirely. Once the system is discretized in time, the endpoint conditions become coordinate constraints on the first and last time-slices, which can be enforced simply by freezing those degrees of freedom. This avoids the need to solve auxiliary boundary-value problems across the entire time interval, and motivates the fully discrete approach developed in the next section.

2.2. The HRF Method for Time-Dependent MFGs. This subsection develops an HRF for a time-discretization of the MFG system (1.1). We first discretize (1.1) and then construct a continuous-time flow for the resulting finite-dimensional problem. After discretization, we enforce the end-point conditions by fixing the boundary slices and evolving only the interior variables, while the density variables evolve on a feasible manifold determined by the slice-wise mass constraints and positivity requirement. On this manifold, we introduce a Riemannian metric induced by a strictly convex entropy. The resulting flow preserves positivity and mass of the density by construction. We discretize (1.1) using the finite-difference scheme of [2]. Existence and uniqueness of the discretized MFG are established in [2].

For clarity, we present the construction on the two-dimensional torus \mathbb{T}^2 using a uniform periodic grid

$$\mathbb{T}_h^2 := \{x_{i,j} = (ih, jh) : i, j = 0, \dots, N_h - 1\}, \quad h := \frac{1}{N_h}, \quad N_x := |\mathbb{T}_h^2| = N_h^2,$$

with periodic indexing. A grid function $y \in \mathbb{R}^{N_x}$ is identified with its values $y_{i,j} := y(x_{i,j})$. We use one-sided differences

$$(D_1^+ y)_{i,j} := \frac{y_{i+1,j} - y_{i,j}}{h}, (D_1^- y)_{i,j} := \frac{y_{i,j} - y_{i-1,j}}{h}, (D_2^+ y)_{i,j} := \frac{y_{i,j+1} - y_{i,j}}{h}, (D_2^- y)_{i,j} := \frac{y_{i,j} - y_{i,j-1}}{h}, \quad (2.6)$$

and the standard five-point Laplacian

$$(\Delta_h y)_{i,j} := -\frac{4y_{i,j} - y_{i+1,j} - y_{i-1,j} - y_{i,j+1} - y_{i,j-1}}{h^2}. \quad (2.7)$$

At each grid node, we collect the four one-sided slopes into the upwind stencil

$$[D_h y]_{i,j} := \left((D_1^+ y)_{i,j}, (D_1^- y)_{i+1,j}, (D_2^+ y)_{i,j}, (D_2^- y)_{i,j+1} \right)^\top \in \mathbb{R}^4. \quad (2.8)$$

Following [2], we approximate the Hamiltonian H in (1.1) by a numerical Hamiltonian

$$g : \mathbb{T}^2 \times \mathbb{R}^4 \rightarrow \mathbb{R}.$$

To keep the notation simple, for each grid node (i, j) we write $g_{i,j}(q) := g(x_{i,j}, q)$ for $q \in \mathbb{R}^4$. Throughout, we assume that H is strictly convex in its momentum argument, and we impose the standard assumptions on g from [2] to preserve this convexity structure at the discrete level.

Assumption 2.1 (Numerical Hamiltonian). *Let $H : \mathbb{T}^2 \times \mathbb{R}^2 \rightarrow \mathbb{R}$ be a continuous Hamiltonian, and assume that for each fixed $x \in \mathbb{T}^2$, the map $p \mapsto H(x, p)$ is strictly convex. Let $g : \mathbb{T}^2 \times \mathbb{R}^4 \rightarrow \mathbb{R}$ be a numerical Hamiltonian, and write $q = (q_1, q_2, q_3, q_4) \in \mathbb{R}^4$. The following properties hold.*

- *Consistency.* For all $x \in \mathbb{T}^2$ and all $\xi_1, \xi_2 \in \mathbb{R}$, $g(x, \xi_1, \xi_1, \xi_2, \xi_2) = H(x, (\xi_1, \xi_2))$.
- *Monotonicity in upwind inputs.* For each fixed $x \in \mathbb{T}^2$, the map $q \mapsto g(x, q)$ is nonincreasing in q_1 and q_3 and nondecreasing in q_2 and q_4 .
- *Regularity and strict convexity.* For each fixed $x \in \mathbb{T}^2$, the map $q \mapsto g(x, q)$ is continuously differentiable and strictly convex on \mathbb{R}^4 .

We discretize the transport operator $-\operatorname{div}(D_p H(\cdot, \nabla u) m)$ in divergence form using the fluxes induced by g . Given $U \in \mathbb{R}^{N_x}$, define

$$\alpha^{(\ell)}(U)_{i,j} := \frac{\partial g_{i,j}}{\partial q_\ell} \left([D_h U]_{i,j} \right), \quad \ell = 1, 2, 3, 4.$$

For $U, M \in \mathbb{R}^{N_x}$, define the discrete transport operator $\mathcal{B}_h(U, M) \in \mathbb{R}^{N_x}$ componentwise by

$$(\mathcal{B}_h(U, M))_{i,j} := -\left(D_1^- (M \alpha^{(1)}(U)) \right)_{i,j} - \left(D_1^+ (M \alpha^{(2)}(U)) \right)_{i,j} - \left(D_2^- (M \alpha^{(3)}(U)) \right)_{i,j} - \left(D_2^+ (M \alpha^{(4)}(U)) \right)_{i,j}, \quad (2.9)$$

where all products are understood pointwise on the grid. For the reader's convenience, we recall in Lemma A.1 the classical discrete result from [2] that, for fixed U , the discrete transport operator $\mathcal{B}_h(U, \cdot)$ is the adjoint of the linearization of the discrete Hamiltonian block at U .

We discretize $[0, T]$ by a uniform grid $0 = t_0 < t_1 < \dots < t_{N_T} = T$ with $\Delta t := T/N_T$. For each $k = 0, \dots, N_T$, we represent the functions on the grid at the time slices by vectors

$$M_k \in \mathbb{R}^{N_x}, \quad U_k \in \mathbb{R}^{N_x}, \quad (M_k)_{i,j} \approx m(x_{i,j}, t_k), \quad (U_k)_{i,j} \approx u(x_{i,j}, t_k).$$

The mixed end-point conditions are imposed by sampling the prescribed initial density $m_0(\cdot)$ and terminal value $u_T(\cdot)$ on the grid:

$$(M_0)_{i,j} := m_0(x_{i,j}), \quad (U_{N_T})_{i,j} := u_T(x_{i,j}).$$

We use the discrete pairing $\langle a, b \rangle_h := h^2 \sum_{i,j} a_{i,j} b_{i,j}$, and since sampling does not in general preserve mass exactly, we enforce $\langle M_0, \mathbf{1} \rangle_h = 1$ by the renormalization

$$M_0 \leftarrow \frac{M_0}{\langle M_0, \mathbf{1} \rangle_h},$$

where $\mathbf{1} \in \mathbb{R}^{N_x}$ is the all-ones vector. We then impose slice-wise mass conservation in the discrete form

$$\langle M_k, \mathbf{1} \rangle_h = 1, \quad k = 0, 1, \dots, N_T. \quad (2.10)$$

We discretize the spatial cost by sampling $V(\cdot)$ on the grid and writing $V_h \in \mathbb{R}^{N_x}$ with $(V_h)_{i,j} := V(x_{i,j})$. The coupling f is applied componentwise to grid densities, and we adopt the following discrete analogue of the Lasry–Lions monotonicity condition.

Assumption 2.2 (Coupling monotonicity). *The function $f : (0, \infty) \rightarrow \mathbb{R}$ is locally Lipschitz and strictly monotone increasing. Equivalently, for any $M, \widetilde{M} \in \mathbb{R}_{++}^{N_x}$ with $M \neq \widetilde{M}$,*

$$\langle f(M) - f(\widetilde{M}), M - \widetilde{M} \rangle_h > 0,$$

where $f(\cdot)$ is applied componentwise.

Since the end-point slices (M_0, U_{N_T}) are fixed, the discrete problem is naturally parametrized by the interior unknowns

$$Y := (M_1, \dots, M_{N_T}, U_0, \dots, U_{N_T-1}) \in \mathcal{X}_h := \left(\mathbb{R}^{N_x} \right)^{N_T} \times \left(\mathbb{R}^{N_x} \right)^{N_T}.$$

Define the open simplex

$$\mathcal{M}_{++ , h} := \left\{ M \in \mathbb{R}^{N_x} : M > 0 \text{ componentwise, } \langle M, \mathbf{1} \rangle_h = 1 \right\}.$$

The feasible set is the endpoint constraint manifold

$$\mathcal{M}_h := \left\{ Y \in \mathcal{X}_h : M_k \in \mathcal{M}_{++ , h} \text{ for } k = 1, \dots, N_T \right\}, \quad (2.11)$$

where the fixed data (M_0, U_{N_T}) are understood as above and used whenever they appear in the residuals.

For $k = 1, \dots, N_T$ we define $r_k(Y) \in \mathbb{R}^{N_x}$ and $s_k(Y) \in \mathbb{R}^{N_x}$ componentwise by

$$(r_k(Y))_{i,j} := \frac{(U_k - U_{k-1})_{i,j}}{\Delta t} + \nu (\Delta_h U_{k-1})_{i,j} - g_{i,j}([D_h U_{k-1}]_{i,j}) + f((M_k)_{i,j}) + (V_h)_{i,j}, \quad (2.12)$$

$$(s_k(Y))_{i,j} := \frac{(M_k - M_{k-1})_{i,j}}{\Delta t} - \nu (\Delta_h M_k)_{i,j} + (\mathcal{B}_h(U_{k-1}, M_k))_{i,j}, \quad (2.13)$$

where M_{k-1} is interpreted as M_0 when $k = 1$, and U_k is interpreted as U_{N_T} when $k = N_T$. We collect the residual blocks into

$$F_h(Y) := (r_1(Y), \dots, r_{N_T}(Y), s_1(Y), \dots, s_{N_T}(Y)) \in \mathcal{Y}_h. \quad (2.14)$$

Solving the fully discretized MFG corresponds to finding $Y \in \mathcal{M}_h$ such that $F_h(Y) = 0$. In the following proposition, we establish the monotonicity of the discrete operator F_h in (2.14).

Proposition 2.1 (Strict monotonicity of F_h). *Assume that the numerical Hamiltonian g satisfies Assumption 2.1 and that the coupling f satisfies Assumption 2.2. Let Y and \widetilde{Y} be two feasible states with the same fixed end-point samples (M_0, U_{N_T}) . Then F_h in (2.14) is strictly monotone with respect to the space-time pairing $\langle \cdot, \cdot \rangle_{h, \Delta t}$, namely*

$$\left\langle F_h(Y) - F_h(\widetilde{Y}), Y - \widetilde{Y} \right\rangle_{h, \Delta t} > 0 \quad \text{for all } Y \neq \widetilde{Y}. \quad (2.15)$$

Next, we build the HRF dynamics on \mathcal{M}_h by endowing it with a Riemannian metric generated by a strictly convex entropy functional. We first introduce the space-time pairing

$$\langle \Xi, \Psi \rangle_{h, \Delta t} := \Delta t \sum_{k=1}^{N_T} \langle \Xi_{M_k}, \Psi_{M_k} \rangle_h + \Delta t \sum_{k=0}^{N_T-1} \langle \Xi_{U_k}, \Psi_{U_k} \rangle_h,$$

for $\Xi, \Psi \in \mathcal{Y}_h$. With respect to this pairing, for $Y = (M_1, \dots, M_{N_T}, U_0, \dots, U_{N_T-1}) \in \mathcal{M}_h$, define

$$\mathcal{E}(Y) := \Delta t \sum_{k=1}^{N_T} \langle M_k, \log M_k - \mathbf{1} \rangle_h + \frac{\Delta t}{2} \sum_{k=0}^{N_T-1} \langle U_k, U_k \rangle_h. \quad (2.16)$$

where $\log M_k$ is understood componentwise and $\mathbf{1} \in \mathbb{R}^{N_x}$ denotes the vector of ones.

We write $\nabla \mathcal{E}(Y)$ and $\nabla^2 \mathcal{E}(Y)$ for the gradient and Hessian of \mathcal{E} with respect to the pairing $\langle \cdot, \cdot \rangle_{h, \Delta t}$, namely

$$D\mathcal{E}(Y)[\Xi] = \langle \nabla \mathcal{E}(Y), \Xi \rangle_{h, \Delta t}, \quad \text{and} \quad D^2\mathcal{E}(Y)[\Xi, \Psi] = \langle \nabla^2 \mathcal{E}(Y) \Xi, \Psi \rangle_{h, \Delta t}.$$

A direct computation shows that

$$\nabla^2 \mathcal{E}(Y) = \text{diag}(1/M_1, \dots, 1/M_{N_T}, I, \dots, I),$$

where $1/M_k$ is understood componentwise.

We then define the Riemannian metric on \mathcal{M}_h by

$$g_{Y, \mathcal{E}}(\Xi, \Psi) := \langle \nabla^2 \mathcal{E}(Y) \Xi, \Psi \rangle_{h, \Delta t}.$$

Here $\Xi_{M_k}, \Psi_{M_k} \in \mathbb{R}^{N_x}$ and $\Xi_{U_k}, \Psi_{U_k} \in \mathbb{R}^{N_x}$ denote the density and value-function components of $\Xi, \Psi \in \mathcal{X}_h$, respectively. The admissible velocity space is

$$\mathcal{T}_{Y, \mathcal{E}} := \left\{ \Xi \in \mathcal{X}_h : \langle \Xi_{M_k}, \mathbf{1} \rangle_h = 0 \text{ for } k = 1, \dots, N_T \right\}.$$

The HRF is defined as

$$\dot{Y}(s) \in \arg \min_{\Xi \in \mathcal{T}_{Y(s), \mathcal{E}}} \left\{ \frac{1}{2} g_{Y(s), \mathcal{E}}(\Xi, \Xi) + \langle F_h(Y(s)), \Xi \rangle_{h, \Delta t} \right\}, \quad Y(0) \in \mathcal{M}_h. \quad (2.17)$$

The mass constraint enters (2.17) through $\mathcal{T}_{Y, \mathcal{E}}$. Because the metric is diagonal in the density blocks and the constraints are linear, the minimizer in (2.17) admits a closed form.

Proposition 2.2 (Explicit Discrete HRF). *For a feasible Y with $M_k \in \mathcal{M}_{+, h}$, $\forall k = 1, \dots, N_T$, define*

$$\bar{r}_k(Y) := \frac{\langle M_k, r_k(Y) \rangle_h}{\langle M_k, \mathbf{1} \rangle_h}, \quad (2.18)$$

The minimizer in (2.17) is unique, and the flow $Y(s)$ satisfies

$$\begin{aligned} \dot{M}_k &= -M_k \odot (r_k(Y(s)) - \bar{r}_k(Y(s)) \mathbf{1}), & k = 1, \dots, N_T, \\ \dot{U}_{k-1} &= -s_k(Y(s)), & k = 1, \dots, N_T, \end{aligned} \quad (2.19)$$

where \odot denotes componentwise multiplication.

Next, we establish global existence for (2.19) together with positivity and mass preservation. Our argument starts from the standard well-posedness theory for ODEs, which requires the following assumption.

Assumption 2.3. *Assume that $V_h \in \mathbb{R}^{N_x}$ is bounded. Assume also that $g : \mathbb{T}^2 \times \mathbb{R}^4 \rightarrow \mathbb{R}$ is continuous in x , differentiable in q , and that $\nabla_q g(x, \cdot)$ is locally Lipschitz in q , uniformly in x .*

The following proposition shows that the HRF remains on the feasible manifold for all flow times.

Proposition 2.3 (Global Existence, Positivity, and Mass Preservation). *Suppose that Assumptions 2.1, 2.2, and 2.3 hold. Let $Y(0) \in \mathcal{M}_h$ be feasible and let $Y(\cdot)$ be the solution of (2.19) with initial datum $Y(0)$. Assume that there exists $Y^* \in \mathcal{M}_h$ such that $F_h(Y^*) = 0$. Then the solution exists for all $s \geq 0$ and satisfies*

$$M_k(s) \in \mathcal{M}_{+, h} \quad \text{for all } s \geq 0, \quad k = 1, \dots, N_T.$$

Meanwhile, $\langle M_k(s), \mathbf{1} \rangle_h = 1$ and $M_k(s) > 0$ componentwise for all $s \geq 0$ and all $k = 1, \dots, N_T$.

The next theorem summarizes the global convergence guarantee.

Theorem 2.4 (Global convergence of the HRF). *Suppose that Assumptions 2.1, 2.2, and 2.3 hold. Let $Y^* \in \mathcal{M}_h$ be a feasible equilibrium such that $F_h(Y^*) = 0$. Let $Y(\cdot)$ be the global solution of (2.19) with feasible initial datum $Y(0) \in \mathcal{M}_h$. Then the Bregman divergence $D_{\mathcal{E}}(Y^*, Y(s))$ is nonincreasing on $[0, \infty)$, and*

$$F_h(Y(s)) \rightarrow 0 \text{ and } Y(s) \rightarrow Y^* \quad \text{as } s \rightarrow \infty.$$

Theorem 2.4 shows that, under the standard Lasry–Lions monotonicity condition, convergence of the HRF does not depend on the initialization. For the numerical experiments in Section 4, we discretize (2.19) in the flow variable using the implicit Euler method.

3. A SOLVER-AGNOSTIC FRAMEWORK FOR INVERSE PROBLEMS

This section introduces a solver-agnostic optimization framework for inverse problems in MFGs. We illustrate the approach on the stationary and time-dependent MFG models in (1.2) and (1.1). The main task is to infer m , u , and the spatial cost V (as well as the ergodic constant λ in the stationary setting) from noisy measurements of m and V .

We formulate the inverse problem in a state-eliminated form. The outer optimization variable is V , constrained to satisfy prescribed regularity assumptions and to fit the available observations. For each candidate V , the corresponding equilibrium state (m, u) (and λ in the stationary case) is defined implicitly as the solution of the associated MFG system. This differs from approaches that treat (m, u, λ, V) as independent decision variables in a single optimization problem. The state-eliminated formulation ensures that, for any sufficiently smooth V , the recovered state automatically satisfies the MFG equations, so the outer optimization operates on the physically consistent manifold of equilibria.

A standard implementation updates the unknown coefficients V by a gradient-based method. However, computing the gradient of the outer objective with respect to V by differentiating through a forward solver can be expensive and tightly coupled to the particular numerical method used to solve the MFG system. Instead, we treat the discrete MFG system as the defining constraint for the MFG state (m, u) and compute the gradient of the outer objective with respect to V by implicit differentiation of these constraints. This yields adjoint-type problems whose solutions provide the desired gradients without unrolling or differentiating through the internal iterations of the forward solver. Building on this implicit differentiation framework, we further derive a GN method that incorporates second-order information to accelerate the outer optimization.

3.1. Stationary and Time-Dependent Inverse Problems. We begin by formulating the inverse problems associated with stationary and time-dependent MFGs.

3.1.1. Inverse Problem for Stationary MFGs. For ease of presentation, we consider the prototype MFG system (1.2). Here, we consider an inverse problem in which we infer both the agents' equilibrium strategies and the spatial cost from limited, noisy observations of the population distribution and the cost. Specifically, we consider the following problem.

Problem 1 (Stationary MFG Inverse Problem). *Given a spatial cost function V^* and known components (H, v, f) , suppose that the stationary MFG (1.2) admits a unique classical solution (u^*, m^*, λ^*) . Assume further that, in practice, we only have noisy observations of m^* and V^* at a finite number of points, and our aim is to recover the full configuration $(u^*, m^*, \lambda^*, V^*)$.*

More precisely, we assume:

1. **Noisy partial observations of m^* .** Let $\{\phi_\ell^o\}_{\ell=1}^{N_m}$ be linear observation functionals. We observe the vector

$$\mathbf{m}^o := (\langle \phi_1^o, m^* \rangle, \dots, \langle \phi_{N_m}^o, m^* \rangle) + \epsilon_m \in \mathbb{R}^{N_m},$$

where $\epsilon_m \in \mathbb{R}^{N_m}$ is a Gaussian noise vector satisfying $\epsilon_m \sim \mathcal{N}(\mathbf{0}, \gamma_m^2 I_{N_m})$. Here $\gamma_m > 0$ denotes the noise standard deviation, I_{N_m} is the $N_m \times N_m$ identity matrix.

2. **Noisy partial observations of V^* .** Let $\{\psi_\ell^o\}_{\ell=1}^{N_v}$ be linear observation functionals acting on V^* . We observe

$$\mathbf{V}^o := (\langle \psi_1^o, V^* \rangle, \dots, \langle \psi_{N_v}^o, V^* \rangle) + \epsilon_v \in \mathbb{R}^{N_v},$$

where $\epsilon_v \in \mathbb{R}^{N_v}$ and $\epsilon_v \sim \mathcal{N}(\mathbf{0}, \gamma_v^2 I_{N_v})$, with $\gamma_v > 0$.

Inverse Problem. Assuming that the agents are governed by the stationary MFG (1.2), and given the noisy data \mathbf{m}^o and \mathbf{V}^o , our goal is to recover the full configuration $(u^*, m^*, \lambda^*, V^*)$.

The above inverse problem is posed in the continuous setting. For computation, we discretize the MFG system and work with the corresponding discrete unknowns and observations. For illustration, we work on the two-dimensional torus \mathbb{T}^2 and discretize the MFG using the standard finite-difference scheme of [2], as described in Section 2.2 and [28]. Let \mathbb{T}_h^2 be the toroidal grid with mesh size h and periodic indices, and let $N_x := |\mathbb{T}_h^2|$. For a grid function $y \in \mathbb{R}^{N_x}$, identified with the nodal values $(y_{i,j})$, we use the same one-sided difference operators, discrete gradient stencil, and standard five-point Laplacian as defined in (2.6), (2.8), and (2.7). Let $g(x, q)$ be a Godunov numerical Hamiltonian approximating $H(x, p)$, with partial derivatives g_{q_k} evaluated at $(x_{i,j}, [D_h U]_{i,j})$. Sampling the fields pointwise on \mathbb{T}_h^2 , we represent

$$M \in \mathbb{R}^{N_x} \approx m(\cdot), \quad U \in \mathbb{R}^{N_x} \approx u(\cdot), \quad V_h \in \mathbb{R}^{N_x} \approx V(\cdot).$$

Define the stationary residual blocks

$$\mathcal{R}_{i,j}^{(m)}(M, U; V_h, \lambda) := \nu(\Delta_h U)_{i,j} - g(x_{i,j}, [D_h U]_{i,j}) + f(M_{i,j}) + (V_h)_{i,j} + \lambda,$$

$$\mathcal{R}_{i,j}^{(u)}(M, U) := -\nu(\Delta_h M)_{i,j} - \left(D_1^-(M g_{q_1})\right)_{i,j} - \left(D_1^+(M g_{q_2})\right)_{i,j} - \left(D_2^-(M g_{q_3})\right)_{i,j} - \left(D_2^+(M g_{q_4})\right)_{i,j}.$$

We use the discrete inner product $\langle a, b \rangle_h := h^2 \sum_{i,j} a_{i,j} b_{i,j}$. The ergodic constant λ is eliminated by enforcing the discrete compatibility condition $\langle M, \mathcal{R}^{(m)}(M, U; V, \lambda) \rangle_h = 0$, i.e.

$$\lambda(M, U, V_h) = -\frac{\langle M, \nu \Delta_h U - g(\cdot, [D_h U]) + f(M) + V_h \rangle_h}{\langle M, \mathbf{1} \rangle_h}.$$

We then define the discrete stationary MFG residual operator

$$F_h(M, U, V_h) := (\mathcal{R}^{(u)}(M, U), \mathcal{R}^{(m)}(M, U; V_h, \lambda(M, U, V_h))) \in \mathbb{R}^{N_x} \times \mathbb{R}^{N_x},$$

together with the normalization constraints

$$\langle M, \mathbf{1} \rangle_h = 1, \quad \langle U, \mathbf{1} \rangle_h = 0.$$

Hence, for a given V_h , the discrete forward problem is to find (M, U) such that

$$F_h(M, U, V_h) = 0, \quad \langle M, \mathbf{1} \rangle_h = 1, \quad \langle U, \mathbf{1} \rangle_h = 0. \quad (3.1)$$

The inverse problem is intrinsically ill-posed: finitely many noisy observations do not determine a unique spatial cost or equilibrium state without additional regularization. We therefore incorporate continuous priors on (m, u, V) while keeping the forward MFG solve fully discrete. A convenient and flexible way to encode smoothness and structural assumptions is to place m , u , and V in reproducing kernel Hilbert spaces (RKHSs) [50], whose norms provide quadratic regularizers and whose evaluation functionals are continuous. This choice also provides a systematic link between the discrete unknowns on \mathbb{T}_h^2 and continuous objects on \mathbb{T}^2 . The grid vectors (M, U, V_h) are interpreted as nodal samples of RKHS functions and are lifted to continuous functions through kernel reconstruction. In this way, continuous observation functionals can be applied consistently to the discretized variables. Thus, we assume that $m \in \mathcal{M}$, $u \in \mathcal{U}$, and $V \in \mathcal{V}$, where \mathcal{M} , \mathcal{U} , and \mathcal{V} are RKHSs on \mathbb{T}^2 with kernels K_m , K_u , and K_V , respectively. Then, we use the standard optimal-recovery reconstruction. Fix a positive definite kernel K on \mathbb{T}^2 with RKHS \mathcal{H}_K , and let $X = \{x_\ell\}_{\ell=1}^{N_x} \subset \mathbb{T}^2$ denote the grid points. Given nodal values $Z \in \mathbb{R}^{N_x}$, we define $\mathcal{R}_h^K(Z) \in \mathcal{H}_K$ as the unique minimizer of

$$\min_{w \in \mathcal{H}_K} \|w\|_{\mathcal{H}_K}^2, \quad \text{such that } w(x_\ell) = Z_\ell, \quad \ell = 1, \dots, N_x. \quad (3.2)$$

By the representer theorem [50], the minimizer has the closed form

$$\mathcal{R}_h^K(Z)(x) = K(x, X)K(X, X)^{-1}Z, \quad x \in \mathbb{T}^2,$$

where $K(X, X) \in \mathbb{R}^{N_x \times N_x}$ is the Gram matrix and $K(x, X) \in \mathbb{R}^{1 \times N_x}$ is the row vector of kernel evaluations at x . Thus, given the grid values M, U , and V_h corresponding to m, u , and V , respectively, we reconstruct continuous representatives via

$$m^\dagger := \mathcal{R}_h^{K_m}(M) \in \mathcal{M}, \quad u^\dagger := \mathcal{R}_h^{K_u}(U) \in \mathcal{U}, \quad V^\dagger := \mathcal{R}_h^{K_V}(V_h) \in \mathcal{V}.$$

Moreover, the RKHS norm of the reconstructed V^\dagger admits an explicit expression, i.e.,

$$\|V^\dagger\|_{\mathcal{V}}^2 = \langle V^\dagger, V^\dagger \rangle_{\mathcal{V}} = V_h^\top K_V(X, X)^{-1} V_h,$$

where $\langle \cdot, \cdot \rangle_{\mathcal{V}}$ denotes the inner product in the RKHS \mathcal{V} associated with the kernel K_V . In practice, $V_h^\top (K_V(X, X) + \epsilon I)^{-1} V_h$ is used with $\epsilon > 0$ for numerical stability.

Using these reconstructions, we can apply the linear observation functionals stated in Problem 1 to the continuous surrogates, rather than restricting observations to the uniform grid \mathbb{T}_h^2 . We define the induced observation maps

$$\Phi_h^m(M) := (\langle \phi_1^o, m^\dagger \rangle, \dots, \langle \phi_{N_m}^o, m^\dagger \rangle) \in \mathbb{R}^{N_m}, \quad \Phi_h^V(V) := (\langle \psi_1^o, V^\dagger \rangle, \dots, \langle \psi_{N_v}^o, V^\dagger \rangle) \in \mathbb{R}^{N_v}.$$

The stationary inverse problem is then formulated as the PDE-constrained optimization problem

$$\min_{V_h \in \mathbb{R}^{N_x}} \frac{\alpha}{2} \|V^\dagger\|_{\mathcal{V}}^2 + \frac{\beta}{2} \|\Phi_h^m(M) - \mathbf{m}^o\|_2^2 + \frac{\gamma}{2} \|\Phi_h^V(V) - \mathbf{V}^o\|_2^2 \quad \text{s.t.} \quad (M, U) \text{ satisfies (3.1)}, \quad (3.3)$$

where $\alpha, \beta, \gamma > 0$ are penalty parameters, and λ is understood as $\lambda(M, U, V_h)$ defined above.

Remark 3.1 (RKHS surrogates for continuous observations). *In Problem 1, observations are formulated as continuous linear functionals acting on the underlying fields (e.g., m and V), whereas the forward MFG solve produces only grid unknowns such as (M, U, V_h) . To apply continuous observation functionals to these discrete outputs, we introduce continuous representatives of the grid data. A standard alternative is a finite-element type reconstruction (e.g., piecewise polynomial interpolation). Here we instead use optimal recovery (3.2).*

This choice is convenient because it provides a systematic, kernel-parameterized family of smooth function classes in which general linear observations are well defined. Moreover, for common kernel families on \mathbb{T}^2 (in particular Matérn kernels), the associated RKHS is norm-equivalent to a Sobolev space $H^s(\mathbb{T}^2)$ for some $s > 0$ (see, e.g., [54]). In particular, choosing s above the Sobolev embedding threshold (e.g., $s > 1$ in two dimensions) ensures that elements admit continuous representatives, so pointwise and other continuous observations are meaningful, and the resulting regularity is consistent with the smoothness typically assumed for classical MFG solutions.

We emphasize that the RKHS assumption is not required by the discrete forward solve itself. The time-dependent inverse formulation adopts the same viewpoint, and we do not repeat this discussion there. \square

3.1.2. Inverse Problem for Time-Dependent MFGs. We now formulate the analogous inverse problem for the time-dependent MFG (1.1).

Problem 2 (Time-Dependent MFG Inverse Problem). *Let V^* be a spatial cost and suppose that the components (H, ν, f, m_0, u_T) are known. For a given V^* , assume the time-dependent MFG system (1.1) admits a unique classical solution (u^*, m^*) . In practice, suppose we have access to partial and noisy observations of m^* and V^* and wish to reconstruct the full configuration (u^*, m^*, V^*) . To elaborate, we have*

1. **Noisy partial observations of m^* .** *Let $\{\phi_\ell^o\}_{\ell=1}^{N_m}$ be linear observation functionals and denote*

$$\mathbf{m}^o = (\langle \phi_1^o, m^* \rangle, \dots, \langle \phi_{N_m}^o, m^* \rangle) + \boldsymbol{\epsilon}_m, \quad \boldsymbol{\epsilon}_m \sim \mathcal{N}(0, \gamma_m^2 I).$$

Here $\gamma_m > 0$ is the noise standard deviation and $\langle \cdot, \cdot \rangle$ denotes the data–state pairing.

2. **Noisy partial observations of V^* .** *Let $\{\psi_\ell^o\}_{\ell=1}^{N_v}$ be linear observation functionals for V^* and define*

$$\mathbf{V}^o = (\langle \psi_1^o, V^* \rangle, \dots, \langle \psi_{N_v}^o, V^* \rangle) + \boldsymbol{\epsilon}_v, \quad \boldsymbol{\epsilon}_v \sim \mathcal{N}(0, \gamma_v^2 I),$$

with noise level $\gamma_v > 0$.

Inverse Problem. *Suppose that agents are involved in the time-dependent MFG in (1.1). Given \mathbf{m}^o and \mathbf{V}^o , we want to recover (u^*, m^*, V^*) .*

Similar to the stationary case, we work with a fully discrete formulation for computation. We use a finite difference scheme in Section 2.2. In particular, we use the space-time grid $(\mathbb{T}_h^2, \{t_k\}_{k=0}^{N_T})$. The mixed end-point data are sampled on the grid and fixed as (M_0, U_{N_T}) , and the interior unknowns are collected as

$$Y := (M_1, \dots, M_{N_T}, U_0, \dots, U_{N_T-1}) \in \mathcal{X}_h, \quad V_h \in \mathbb{R}^{N_x}.$$

To make the dependence on V_h explicit, we write the residual operator in (2.14) as $F_h(\cdot; V_h) : \mathcal{X}_h \rightarrow \mathcal{X}_h$. Here $F_h(\cdot; V_h)$ denotes the discrete space-time MFG residual, where the fixed end-point slices (M_0, U_{N_T}) are inserted whenever they appear in the time-slice blocks. The discrete forward constraint is therefore

$$F_h(Y; V_h) = 0, \quad Y \in \mathcal{M}_h, \quad (3.4)$$

with \mathcal{M}_h the feasible end-point manifold defined in Section 2.2.

To apply continuous observation functionals to the discrete unknowns, we construct continuous surrogates from the grid values using kernel optimal recovery. We place the space-time fields m and u in RKHSs on $\mathbb{T}^2 \times [0, T]$ with kernels K_m and K_u , and we place the spatial cost V in an RKHS on \mathbb{T}^2 with kernel K_V . Let $X = \{x_\ell\}_{\ell=1}^{N_x} \subset \mathbb{T}^2$ be the spatial grid points and let $T = \{t_k\}_{k=0}^{N_T}$ be the time grid, and set $S := X \times T$.

For a space-time kernel K and a space-time sample vector $w \in \mathbb{R}^{N_x(N_T+1)}$ (stacked over the space-time grid $S := \{(x_\ell, t_k)\}_{\ell=1, k=0}^{N_x, N_T}$), the analogous optimal-recovery problem to (3.2) yields the representer formula

$$\mathcal{R}_{h, \Delta t}^K(w)(x, t) := K((x, t), S)K(S, S)^{-1}w, \quad (x, t) \in \mathbb{T}^2 \times [0, T].$$

Likewise, for a spatial kernel K and a spatial sample vector $v \in \mathbb{R}^{N_x}$ (stacked over the spatial grid $X := \{x_\ell\}_{\ell=1}^{N_x}$), define

$$\mathcal{R}_h^K(v)(x) := K(x, X)K(X, X)^{-1}v, \quad x \in \mathbb{T}^2.$$

Applying these maps to the discrete unknowns yields the continuous surrogates

$$m^\dagger := \mathcal{R}_{h, \Delta t}^{K_m}(\mathbf{m}_h), \quad u^\dagger := \mathcal{R}_{h, \Delta t}^{K_u}(\mathbf{u}_h), \quad V^\dagger := \mathcal{R}_h^{K_V}(V_h),$$

where $\mathbf{m}_h := (M_0, \dots, M_{N_T}) \in \mathbb{R}^{N_x(N_T+1)}$ and $\mathbf{u}_h := (U_0, \dots, U_{N_T}) \in \mathbb{R}^{N_x(N_T+1)}$ denote the stacked space-time samples. Moreover, V^\dagger satisfies the explicit norm identity

$$\|V^\dagger\|_V^2 = V_h^T K_V(X, X)^{-1}V_h,$$

which follows directly from the representer form.

Using these reconstructions, we can apply the linear observation functionals to the continuous surrogates. We define the induced observation maps

$$\Phi_{h, \Delta t}^m(Y) := (\langle \phi_1^o, m^\dagger \rangle, \dots, \langle \phi_{N_m}^o, m^\dagger \rangle) \in \mathbb{R}^{N_m}, \quad \Phi_h^V(V_h) := (\langle \psi_1^o, V^\dagger \rangle, \dots, \langle \psi_{N_v}^o, V^\dagger \rangle) \in \mathbb{R}^{N_v}.$$

The time-dependent inverse problem is then posed as the PDE-constrained optimization problem

$$\min_{Y \in \mathbb{R}^{N_x}} \frac{\alpha}{2} \|V^\dagger\|_V^2 + \frac{\beta}{2} \|\Phi_{h, \Delta t}^m(Y) - \mathbf{m}^o\|_2^2 + \frac{\gamma}{2} \|\Phi_h^V(V_h) - \mathbf{V}^o\|_2^2 \quad \text{s.t. } Y \text{ satisfies (3.4)}, \quad (3.5)$$

with penalty parameters $\alpha, \beta, \gamma > 0$.

3.2. A Solver-Agnostic Inverse Framework. Our next goal is to solve (3.3) and (3.5) numerically. To this end, we separate the outer optimization from the particular numerical method used for the inner MFG solve. The key idea is to treat the discretized MFG system as the defining constraint for the inner solution: for each parameter value, the inner solver returns an accurate state satisfying the discrete MFG equations, and these equations are the objects we differentiate. Accordingly, derivatives of the outer objective with respect to the unknown parameters are obtained by implicit adjoint differentiation of the discrete MFG constraints, rather than by differentiating through the iterations of a specific inner algorithm. Since (3.3) and (3.5) share the same structure from this viewpoint, we present the method in a unified template.

Let $\theta \in \mathbb{R}^p$ denote the unknown parameter (e.g., a discretized spatial cost), and let $z^*(\theta) \in \mathbb{R}^n$ denote the discrete MFG state associated with θ (e.g., the stacked density and value-function variables, and any auxiliary scalars such as an ergodic constant). In our inverse framework, $z^*(\theta)$ is characterized implicitly as a solution of the discretized MFG,

$$F(z^*(\theta), \theta) = 0, \quad A z^*(\theta) = \mathbf{b}, \quad (3.6)$$

where $F : \mathbb{R}^n \times \mathbb{R}^p \rightarrow \mathbb{R}^n$ is the residual operator induced by the chosen discretization of the coupled MFG equations, and $\mathbf{A} \in \mathbb{R}^{q \times n}$ is a full-row-rank linear operator encoding any additional linear constraints (such as mass normalization, gauge conditions, or boundary data) that are not already incorporated into F .

In the stationary MFG setting, the linear constraints $\mathbf{A}z = \mathbf{b}$ encode standard normalization and gauge conditions. For instance, if $z = (M, U)$ collects the spatial grid unknowns, one may impose

$$\frac{1}{N_x} \sum_i M_i = 1, \quad \sum_i U_i = 0,$$

which can be written compactly in the form $\mathbf{A}z = \mathbf{b}$.

In the time-dependent MFG setting, the mixed endpoint data are imposed after discretization as fixed values on finitely many time slices. Following Section 2.2, we enforce these endpoint constraints by eliminating the fixed endpoint blocks and working only with the interior unknowns. In the resulting reduced system, the endpoint conditions are already built into the parametrization and therefore do not appear as additional explicit equalities. In the abstract form (3.6), this corresponds to the degenerate case $q = 0$, for which the constraint $\mathbf{A}z = \mathbf{b}$ is absent.

We now define a unified objective that matches the formulations in (3.3) and (3.5). Let $z^\circ \in \mathbb{R}^m$ and $\theta^\circ \in \mathbb{R}^r$ denote given data vectors, and let

$$W \in \mathbb{R}^{m \times n}, \quad G \in \mathbb{R}^{r \times p}, \quad J \in \mathbb{R}^{p \times p}$$

be linear maps defining the observation and regularization operators. We consider the objective

$$\mathcal{J}(\theta) = \frac{\alpha}{2} \|J\theta\|_2^2 + \frac{\beta}{2} \|Wz^*(\theta) - z^\circ\|_2^2 + \frac{\gamma}{2} \|G\theta - \theta^\circ\|_2^2, \quad \min_{\theta \in \Theta} \mathcal{J}(\theta), \quad (3.7)$$

with weights $\alpha \geq 0$ and $\beta, \gamma > 0$. In the stationary inverse problem, W represents the discrete observation of the equilibrium density, G represents the discrete observation of the cost V , and J represents the RKHS regularizer. In our setting, the parameter θ is the grid vector V_h corresponding to the spatial cost V . The term $\|J\theta\|_2^2$ is therefore chosen so as to approximate the RKHS norm of the continuous function reconstructed from V_h . Concretely, let X denote the spatial grid, and let $K_V(X, X)$ be the kernel matrix of the reproducing kernel K_V evaluated on X . Then a natural choice is

$$J^\top J = K_V(X, X)^{-1}.$$

Accordingly,

$$\|JV_h\|_2^2 = V_h^\top K_V(X, X)^{-1} V_h,$$

which equals $\|V^\dagger\|_V^2$, where V^\dagger is the RKHS interpolant associated with the grid values V_h .

We solve (3.7) by computing $\nabla_\theta \mathcal{J}(\theta)$ without differentiating through a particular forward solver. The next result provides an adjoint formula that depends only on the discrete system (3.6).

Proposition 3.2. *Assume that F is differentiable in (z, θ) . Let $z^*(\theta)$ satisfy (3.6), and define the adjoint variables $(\psi, \eta) \in \mathbb{R}^n \times \mathbb{R}^q$ as any solution of*

$$\frac{\partial F}{\partial z}(z^*(\theta), \theta)^\top \psi + \mathbf{A}^\top \eta = -\beta W^\top (Wz^*(\theta) - z^\circ), \quad \mathbf{A}\psi = 0, \quad (3.8)$$

with the convention that η and the constraint $\mathbf{A}\psi = 0$ are omitted when $q = 0$. Then the gradient of \mathcal{J} in (3.7) is

$$\nabla_\theta \mathcal{J}(\theta) = \frac{\partial F}{\partial \theta}(z^*(\theta), \theta)^\top \psi + \gamma G^\top (G\theta - \theta^\circ) + \alpha J^\top J\theta. \quad (3.9)$$

With this formulation, computing $\nabla_\theta \mathcal{J}(\theta)$ only requires that the inner solver returns a sufficiently accurate solution $z^*(\theta)$ of the discrete MFG constraints (3.6). No differentiation through the solver itself is needed.

Proposition 3.2 requires solving the linear system (3.8). If $F(\cdot, \theta)$ is strongly monotone in z and the constraint operator \mathbf{A} has full row rank, then (3.8) admits a unique solution, so the adjoint variables are well defined and uniquely determined. For the MFG discretizations considered here, one typically has only strict monotonicity (rather than strong monotonicity), and the linearized system may be singular or ill-conditioned due to near-degeneracy. Nevertheless, in the numerical experiments reported in Section 4, the adjoint solve remains stable, and the resulting gradients yield consistent descent in the outer optimization. We conjecture

that, in practice, the iterates remain in a compact subset of the feasible region where the density is uniformly bounded away from zero. On such a set, the strict monotonicity of F may strengthen to a local strong monotonicity or uniform coercivity property, which would explain the observed stability of the adjoint solve. A rigorous analysis of this mechanism is left for future work. When numerical degeneracy is encountered, one may introduce mild regularization in the adjoint solve. Common choices include computing a minimum-norm adjoint via a least-squares solve, adding a small Tikhonov term (for instance, solving the normal equations with $(\partial_z F)^\top (\partial_z F) + \varepsilon I$), or imposing an additional gauge-fixing condition (such as a zero-mean constraint on the value function) through \mathbf{A} . These modifications are intended to select a well-conditioned adjoint representative in practice.

3.3. Gauss–Newton Method. The adjoint-based gradient formula in Section 3.2 provides a first-order method for minimizing the objective (3.7) with respect to the parameter θ . We also consider a GN method, which exploits the least-squares structure of the objective and typically produces a more effective parameter update than gradient descent (GD).

The equilibrium constraints define the state $z^*(\theta)$ implicitly as a function of θ . Substituting this state into the objective yields the least-squares representation

$$r(\theta) := \begin{bmatrix} \sqrt{\beta} (Wz^*(\theta) - z^o) \\ \sqrt{\gamma} (G\theta - \theta^o) \\ \sqrt{\alpha} J\theta \end{bmatrix}, \quad \mathcal{J}(\theta) = \frac{1}{2} \|r(\theta)\|_2^2, \quad (3.10)$$

where $z^*(\theta)$ satisfies the equilibrium system (3.6).

At a current iterate θ , the GN method computes an increment $p \in \mathbb{R}^p$ by minimizing a quadratic model obtained from the first-order expansion $r(\theta + p) \approx r(\theta) + J_r(\theta)p$, where $J_r(\theta)$ denotes the Jacobian of the residual $r(\theta)$ with respect to θ . Thus, the GN step is defined by the linearized least-squares problem

$$\min_{p \in \mathbb{R}^p} \frac{1}{2} \|r(\theta) + J_r(\theta)p\|_2^2. \quad (3.11)$$

The only subtle point is the evaluation of the Jacobian action $J_r(\theta)p$. Since the residual depends on θ both directly and through the equilibrium state $z^*(\theta)$, one must first determine the first-order change in the equilibrium state induced by the parameter perturbation p . The details of the GN update are given below.

Proposition 3.3 (Gauss–Newton step). *Let $\theta \in \mathbb{R}^p$ be fixed, and let $z^*(\theta) \in \mathbb{R}^n$ satisfy (3.6). For a parameter increment $p \in \mathbb{R}^p$, let $\delta z_p \in \mathbb{R}^n$ denote the associated first-order variation of the equilibrium state, determined by*

$$\frac{\partial F}{\partial z}(z^*(\theta), \theta) \delta z_p + \frac{\partial F}{\partial \theta}(z^*(\theta), \theta) p = 0, \quad \mathbf{A} \delta z_p = 0. \quad (3.12)$$

Then

$$J_r(\theta)p = \begin{bmatrix} \sqrt{\beta} W \delta z_p \\ \sqrt{\gamma} Gp \\ \sqrt{\alpha} Jp \end{bmatrix},$$

and the minimizer of (3.11) is characterized by

$$(J_r(\theta)^\top J_r(\theta))p = -J_r(\theta)^\top r(\theta). \quad (3.13)$$

The proof is given in Appendix A. Once the GN increment p^k has been computed at θ^k , we update

$$\theta^{k+1} = \theta^k + p^k,$$

and then recompute the equilibrium state by solving (3.6) at θ^{k+1} .

In Section 4, we observe that GN typically reaches comparable accuracy in fewer outer iterations than GD. Computationally, the GD method requires solving the adjoint system (3.8) to evaluate the gradient. The GN method instead relies on the sensitivity system (3.12), and its additional cost comes from solving (3.13). This step can be carried out matrix-free using a Krylov method such as conjugate gradients, without explicitly forming $J_r(\theta)^\top J_r(\theta)$.

4. NUMERICAL RESULTS

In this section, we present numerical results for the HRF method and the solver-agnostic inverse framework. We study two solvers for the minimization of the inverse problems. The first is the adjoint-based GD method presented in Section 3.2, which computes gradients via the adjoint method. The second is the GN method presented in Section 3.3. Unless otherwise specified, all forward evaluations employ the HRF with an implicit Euler time discretization. We present experiments on several stationary and time-dependent MFG examples. Two examples are worth highlighting. In Section 4.2.2, we consider a stationary non-potential MFG satisfying the Lasry–Lions monotonicity condition, demonstrating that our framework extends beyond the potential MFG setting. In Section 4.2.3, we apply the same inverse framework with different forward solvers and show that the reconstruction quality remains consistent across solvers, demonstrating the solver-agnostic property of our framework.

We assess the mismatch between the recovered function and a reference function using a discrete L^2 metric. Let u and v be functions on $[a, b]^2$, sampled on a uniform grid with spacings h_x and h_y in the x - and y -directions, producing arrays $\{u_{ij}\}$ and $\{v_{ij}\}$. The discrete L^2 error is defined by

$$\mathcal{E}_2(u, v) := \sqrt{h_x h_y \sum_{i,j} |u_{ij} - v_{ij}|^2}. \quad (4.1)$$

In all experiments, the algorithm terminates when the absolute change in the objective value in (3.7) between two successive iterations falls below 10^{-6} .

4.1. A One-Dimensional Stationary MFG Inverse Problem. In this subsection, we consider the inverse problem for the following one-dimensional stationary MFG posed on the torus \mathbb{T} :

$$\begin{cases} \frac{|P + D_x u|^2}{2} - V(x) = \lambda + \frac{1}{k} \ln m, & x \in \mathbb{T}, \\ -(m(P + D_x u))_x = 0, & x \in \mathbb{T}, \end{cases} \quad (4.2)$$

where $k = 100$, $P = 2$, and the spatial cost is $V(x) = \frac{1}{2}(\sin(\pi x) + \sin(4\pi x))$. The system (4.2) admits a unique smooth solution $(u, m, \lambda) \in C^\infty(\mathbb{T}) \times C^\infty(\mathbb{T}) \times \mathbb{R}$. In this experiment, our objective is to reconstruct u , m , λ , and V in (4.2) from partial noisy observations of m and V .

Experimental Setup. We identify \mathbb{T} with the interval $[0, 1)$. We solve (4.2) using the HRF method of [28] to compute the reference solution (u^*, m^*, λ^*) . The domain \mathbb{T} is discretized with grid spacing $h_x = 1/100$, yielding 100 grid points. We select 8 grid points as observation locations for m and 10 grid points as observation locations for V . The regularization parameters in (3.5) are set to $\alpha = 0.002$, $\beta = 2$, and $\gamma = 2$. We contaminate the observations with i.i.d. Gaussian noise $\mathcal{N}(0, \eta^2 I)$ with $\eta = 10^{-3}$. To solve the inverse problem, we initialize $u \equiv 0$, $m \equiv 1$, and $V \equiv 0$. We then apply the adjoint-based method and the GN method described in Section 3.2 and Section 3.3, respectively.

Experimental Results. Table 1 reports the HRF reference value of λ for (4.2) together with the values recovered by GD and GN. Figure 1 summarizes the numerical results: the HRF reference density m^* is shown in Figure 1a, with the GD and GN reconstructions in Figures 1e and 1i. The same figure also includes the corresponding reference and reconstructed profiles for u and V . Reconstruction errors are reported as pointwise absolute errors, e.g., $|m - m^*|$, with analogous curves for u and V . Finally, Figure 1d compares the outer-level objective in (3.3) and shows that GN converges in substantially fewer iterations than GD.

TABLE 1. Numerical results for λ in the first-order stationary MFG (4.2) using different methods. The reference solution is computed by the HRF [28], and the recovered solution is obtained by the GD method and the GN method.

Method	Reference	GD	GN
λ	1.70043070502	1.70352563486	1.70306872525

4.2. Two-Dimensional Stationary MFG Inverse Problem. In this study, we consider inverse problems for two stationary MFGs: a first-order model with congestion and a non-potential second-order model. We also assess solver-agnostic robustness by varying the inner forward solver used in the inverse problem.

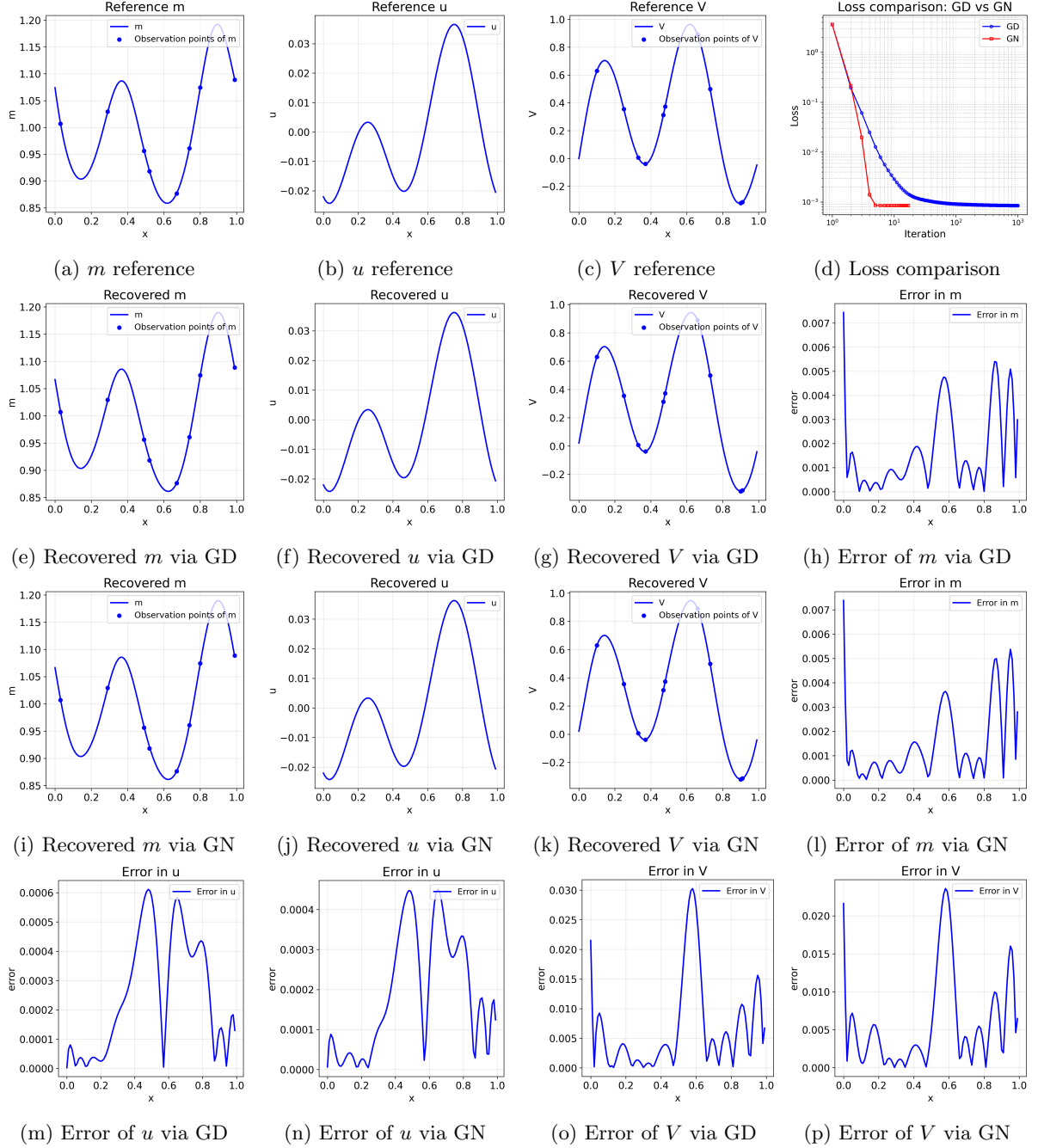


FIG. 1. Numerical results for the inverse problem of the one-dimensional stationary MFG in (4.2). (a), (b), (c) are references for m, u, V ; (d) Log-log plot comparing the GD and GN losses across iterations; (e), (f), (g) recovered m, u, V via GD; (h), (m), (o) errors of m, u, V via GD; (i), (j), (k) recovered m, u, V via GN; (l), (n), (p) errors of m, u, V via GN.

4.2.1. *A First-Order Stationary MFG with Congestion.* Here, we consider the first-order stationary MFG with congestion

$$\begin{cases} H(\nabla u) - V(x, y) = \lambda + m^3, & (x, y) \in \mathbb{T}^2, \\ -\operatorname{div}(D_p H(\nabla u) m) = 0, & (x, y) \in \mathbb{T}^2, \\ \int_{\mathbb{T}^2} u \, dx \, dy = 0, & \int_{\mathbb{T}^2} m \, dx \, dy = 1, \end{cases} \quad (4.3)$$

where $\lambda \in \mathbb{R}$. We take the Hamiltonian $H(p) = \frac{|Q+p|^b}{b m^a}$, $b = 2.0$, $a = 1.5$, $Q = (1, 3)$, and the spatial cost $V(x, y) = 2 \sin\left(2\pi\left(x + \frac{1}{4}\right)\right) \cos\left(2\pi\left(y + \frac{1}{4}\right)\right)$. The system (4.3) admits a unique smooth solution (u, m, λ) . In this example, we study the inverse problem of recovering u , m , V , and λ from partial noisy observations of m and V .

Experimental Setup. We identify \mathbb{T} with the interval $[0, 1)$ and discretize \mathbb{T}^2 using a uniform grid with spacings $h_x = h_y = 1/40$, yielding 1600 grid points. We then sample 128 observation locations for m and 320 observation locations for V independently and uniformly at random from $[0, 1)^2$. The regularization parameters are $\alpha = 0.04$, $\beta = 2$, and $\gamma = 2$. We add i.i.d. Gaussian noise $\mathcal{N}(0, \eta^2 I)$ with $\eta = 10^{-3}$ to the observations. For the inverse problem, we initialize $u \equiv 0$, $m \equiv 1$, and $V \equiv 0$. The reference solution (u^*, m^*, λ^*) is computed by solving (4.3) with the HRF method. We then solve the inverse problem using GD and GN.

Experimental Results. Figures 2a–2b visualize the collocation grid and the selected observation locations for m and V . Figure 3 reports reconstruction accuracy versus the number of observed spatial points, showing systematic decreases in the discrete L^2 errors for m , u , and V as observation density increases. Table 2 compares the HRF reference value of λ with the values recovered by GD and GN. Figure 4 summarizes the inverse-recovery results for (4.3): it includes the HRF reference fields, the GD and GN reconstructions, and the corresponding pointwise absolute error maps for m , u , and V . Finally, Figure 4d shows that GN converges faster than GD.

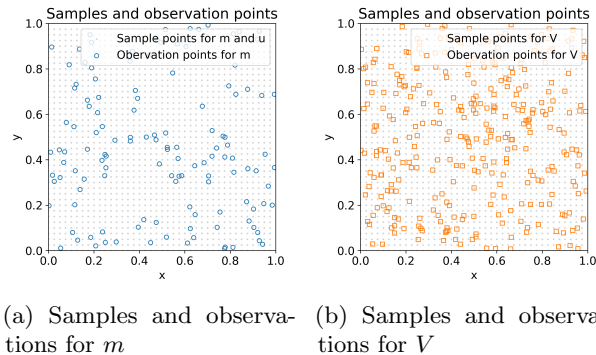


FIG. 2. The inverse problem of the stationary MFG (4.3): samples for m , u and V & corresponding observation points.

TABLE 2. Numerical results for λ in the first-order stationary MFG with congestion problem (4.3) using different methods. The reference solution is computed by the monotone HRF, and the recovered solution is obtained by the GD method and the GN method.

Method	Reference	GD	GN
λ	4.04456433468	4.04563955831	4.04507371305

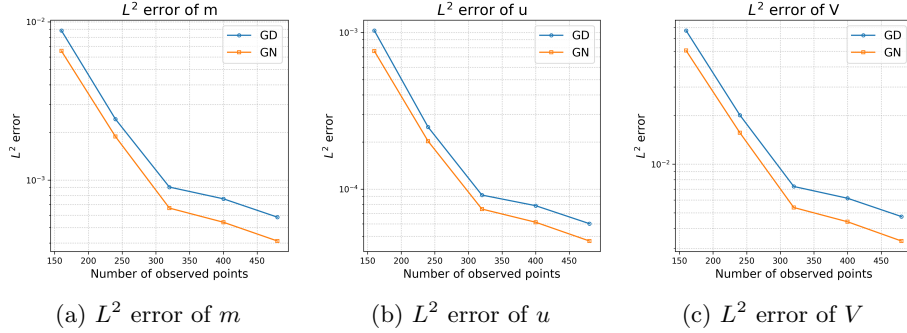


FIG. 3. Numerical results for solving the inverse problem of the MFG system in (4.3) using the adjoint-based GD method and the GN method: (a)-(c) show the L^2 errors for m , u , and V , respectively, versus their exact counterparts as the number of observation points increases.

4.2.2. *A Non-Potential Second-Order Stationary MFG.* Here, we consider the following non-potential stationary MFG on \mathbb{T}^2 :

$$\begin{cases} -\nu\Delta u + \frac{|\nabla u|^2}{2} - V(x, y) = \lambda + f(m), & (x, y) \in \mathbb{T}^2, \\ -\nu\Delta m - \operatorname{div}(m\nabla u) = 0, & (x, y) \in \mathbb{T}^2, \\ \int_{\mathbb{T}^2} u \, dx \, dy = 0, & \int_{\mathbb{T}^2} m \, dx \, dy = 1. \end{cases} \quad (4.4)$$

We take $\nu = 0.1$, $f(m) = m^2 + b(x, y) \cdot \nabla m$, $b(x, y) = (-\sin(2\pi y), \sin(2\pi x))$, and the spatial cost $V(x, y) = -(\sin(2\pi x) + \cos(4\pi x) + \sin(2\pi y))$. Let (u, m, λ) denote the unique solution of (4.4). The inverse problem is to recover (u, m, λ, V) from partial noisy observations of m and V .

Experimental Setup. Let \mathbb{T} be identified by $[0, 1)$. We discretize the spatial domain \mathbb{T}^2 with a grid size $h_x = h_y = \frac{1}{30}$, resulting in 900 total grid points. The observation points are sampled at random: 72 locations for m and 180 locations for V are selected uniformly from $[0, 1)^2$. The regularization parameters are set to $\alpha = 0.04$, $\beta = 1$, $\gamma = 1$. Gaussian noise $\mathcal{N}(0, \eta^2 I)$ with $\eta = 10^{-3}$ is added to the observations. The system is initialized with $u \equiv 0$, $m \equiv 1$, and $V \equiv 0$ for the numerical simulation.

Experimental Results. Figures 5a–5b show the collocation grid and the observation locations for m and V . Table 3 compares the HRF reference value of λ with the values recovered by GD and GN. Figure 6 summarizes the numerical results for (4.4): it includes the HRF reference fields, the GD and GN reconstructions (e.g., m in Panels 6a and Figures 6e–6i), and the corresponding pointwise absolute error maps for m , u , and V . Finally, Figure 6d shows that GN reaches a comparable optimum in fewer iterations than GD and yields more accurate reconstructions.

TABLE 3. Numerical results for λ in the stationary MFG (4.4) using different methods. The reference solution is computed by the HRF, and the recovered solution is obtained by the GD method and the GN method.

Method	Reference	GD	GN
λ	-0.538470584730	-0.543568902915	-0.543101122058

4.2.3. *Solver-Agnostic Property of the Inverse Problem Framework.* To illustrate the solver-agnostic nature of the framework in Section 3, we compare three different inner solvers for (4.4): the HRF [28], Newton-based method [2], and the policy iteration [12]. We compare reconstruction accuracy and convergence behavior across these implementations to validate the robustness of the proposed inverse framework.

Experimental Setup. We consider (4.4) with coupling $f(m) = 50(1 - \Delta)^{-1}(1 - \Delta)^{-1}m$ and spatial cost $V(x, y) = \sin(2\pi x) + \cos(2\pi x) + \sin(4\pi y)$. We set $\nu = 0.2$ and discretize \mathbb{T}^2 with $h_x = h_y = 1/30$. We use 72

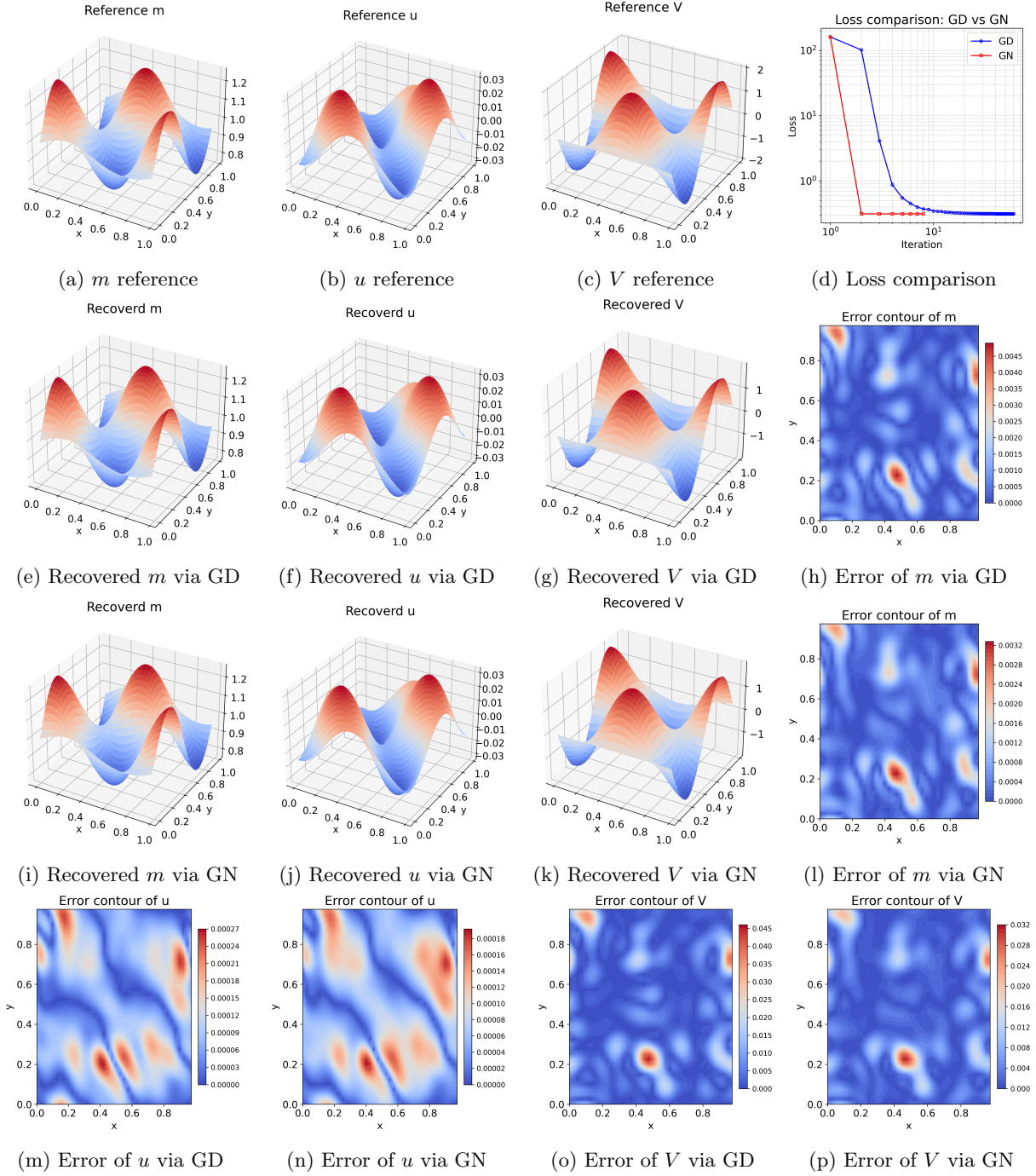


FIG. 4. Numerical results for the inverse problem of the stationary MFG in (4.3). (a), (b), (c) are references for m, u, V ; (d) log-log plot of the loss comparison for GD and GN across iterations; (e), (f), (g) recovered m, u, V via GD; (h), (m), (o) errors of m, u, V via GD; (i), (j), (k) recovered m, u, V via GN; (l), (n), (p) errors of m, u, V via GN.

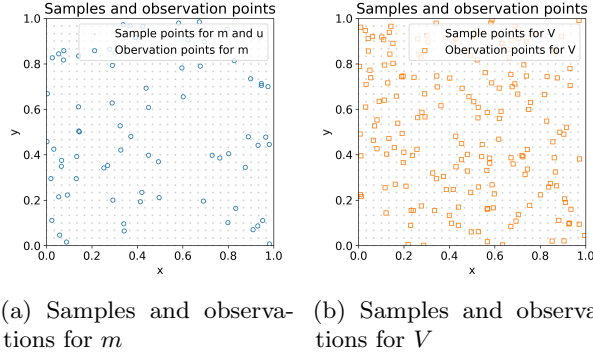


FIG. 5. The inverse problem of the stationary MFG (4.4): samples for m , u and V & corresponding observation points.

observation points for m and 180 for V . The regularization parameters are $\alpha = 0.04$, $\beta = 2$, and $\gamma = 2$, and we add i.i.d. Gaussian noise with level $\eta = 10^{-3}$ to the observations.

Experimental Results. Table 4 reports the discretized L^2 errors of the recovered variables (u, m, V, λ) for three inner MFG solvers and for both outer schemes (GD and GN). Figure 7 shows the corresponding log-log plots of the loss versus iteration under each solver. The comparable accuracy and convergence behavior across all three implementations support the solver-agnostic nature of our framework. In particular, the inner solver can be chosen based on computational resources or implementation constraints without materially affecting reconstruction quality.

TABLE 4. Discretized L^2 recovery errors for the second-order stationary MFG in Section 4.2.3, using different inner MFG solvers.

Inner MFG Solver	Inverse Solver	Error in Variables (L^2)			
		m	u	V	λ
Monotone Flow	GD	1.305434e-03	2.946326e-04	7.805980e-03	1.103745e-03
	GN	1.262210e-03	2.821916e-04	7.552066e-03	1.126094e-03
Newton-based Method	GD	1.411298e-03	3.200899e-04	8.291286e-03	1.136011e-03
	GN	1.262438e-03	2.822591e-04	7.552039e-03	1.126042e-03
Policy Iteration	GD	1.081458e-03	2.259894e-04	6.784161e-03	1.228694e-03
	GN	1.024403e-03	2.122809e-04	6.232931e-03	1.062980e-03

4.3. Time-Dependent MFG Inverse Problems. In this subsection, we consider inverse problems for time-dependent MFGs. Fix $\nu \geq 0$, and choose a Hamiltonian H , a coupling f , a spatial cost V , an initial density m_0 , and a terminal value function u_T . We restrict attention to choices of H , f , V , m_0 , and u_T for which the MFG system below admits a unique smooth solution (u, m) :

$$\begin{cases} -\partial_t u - \nu \Delta u + H(D_x u) - V(x) = f(m), & \forall (x, t) \in \mathbb{T}^d \times (0, T), \\ \partial_t m - \nu \Delta m - \operatorname{div}(D_p H(D_x u) m) = 0, & \forall (x, t) \in \mathbb{T}^d \times (0, T), \\ m(x, 0) = m_0(x), \quad u(x, T) = u_T(x). \end{cases} \quad (4.5)$$

4.3.1. One-Dimensional Time Dependent MFG Inverse Problem. In this example, we set $d = 1$ and specialize (4.5) to the one-dimensional time-dependent MFG setting. We choose the Hamiltonian $H(p) = \frac{1}{2}|p|^2$. We identify \mathbb{T} with $[0, 1)$, set $T = 1$, and take $m_0(\cdot) \equiv 1$ and $u_T(\cdot) \equiv 0$. The coupling is chosen as $f(m) = (1 - \Delta)^{-1}(1 - \Delta)^{-1}m$, and the spatial cost is $V(x) = \sin(2\pi x) + \cos(4\pi x)$. We set the viscosity coefficient to $\nu = 0.1$.

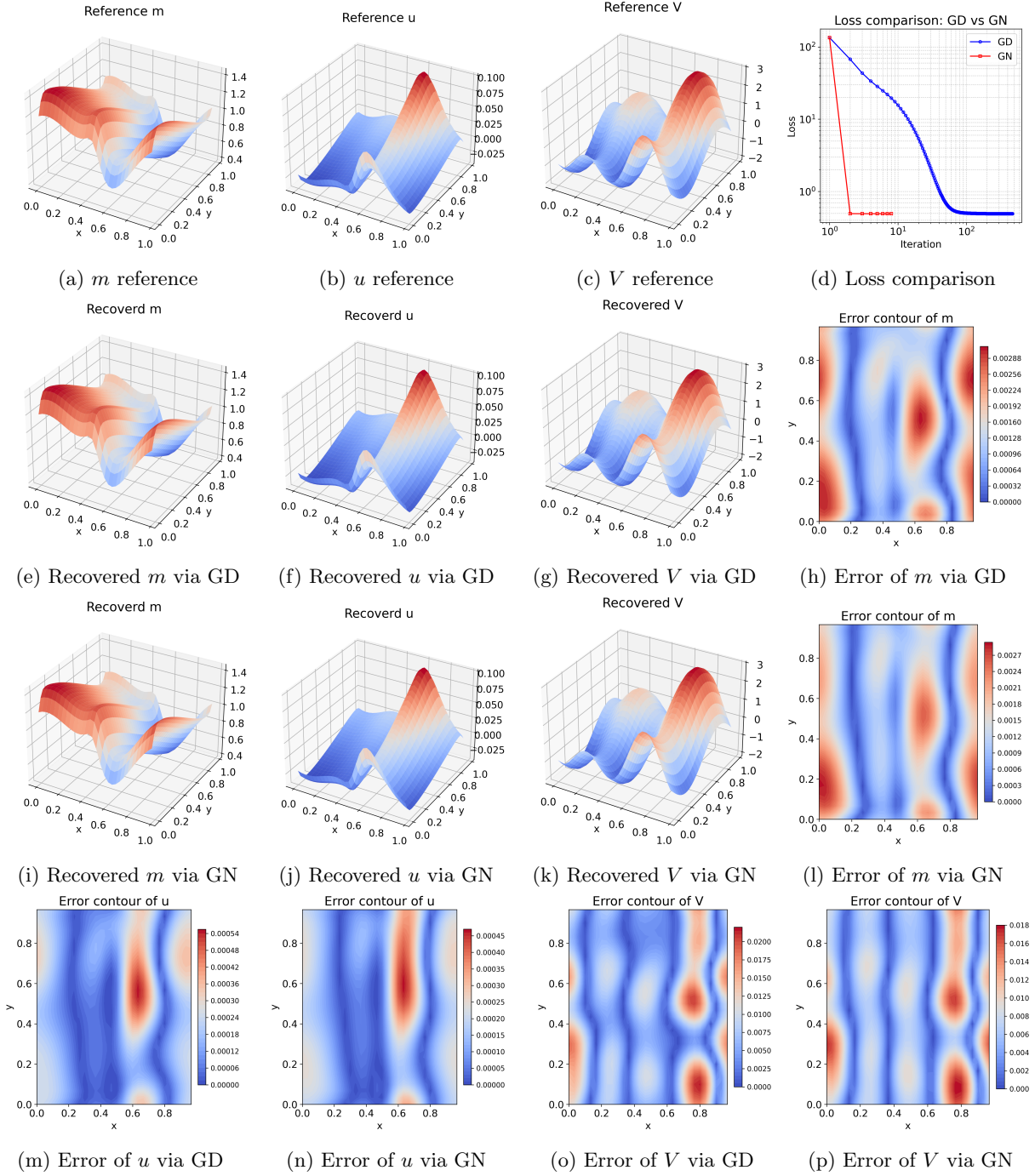


FIG. 6. Numerical results for the inverse problem of the second-order stationary MFG in (4.4). (a), (b), (c) are references for m, u, V ; (d) log-log plot of the loss comparison for GD and GN across iterations; (e), (f), (g) recovered m, u, V via GD; (h), (m), (o) errors of m, u, V via GD; (i), (j), (k) recovered m, u, V via GN; (l), (n), (p) errors of m, u, V via GN.

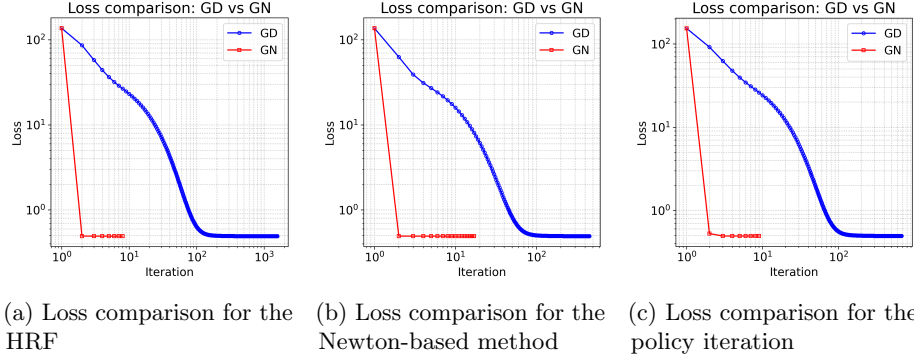


FIG. 7. Log-log plots of the loss versus iteration for GD and GN applied to the inverse problem in Section 4.2.3, using different inner MFG solvers. Panels (a)–(c) correspond to HRF, Newton-based method, and policy iteration, respectively.

Experimental Setup. We discretize the spatial domain \mathbb{T} with grid size $h_x = \frac{1}{40}$ and the time interval $[0, 1]$ with grid size $h_t = \frac{1}{40}$, yielding $40 \times 40 = 1600$ space-time grid points. Among these, 96 points are selected as observations for m . In addition, 10 observation locations for V are selected in the spatial domain. The regularization parameters are set to $\alpha = 0.04$, $\beta = 2$, and $\gamma = 2$. Gaussian noise $\mathcal{N}(0, \eta^2 I)$ with $\eta = 10^{-3}$ is added to the observations. The initial guesses are $u \equiv 0$, $m \equiv 1$, and $V \equiv 0$. Under these specifications, we solve (4.5) using the HRF method introduced in Section 2 to obtain reference solutions (u^*, m^*) . We then consider the inverse problem of recovering u , m , and V from noisy and partial observations of m and V , using the adjoint algorithm and the GN method described in Section 3.

Experimental Results. Figure 8 depicts the collocation grid and the observation locations for m and u . Figure 9 summarizes the reconstruction performance by displaying the reference fields, the reconstructions, and the corresponding pointwise error contours for m , u , and V . Finally, the loss curves in Figure 9d show that the GN method converges markedly faster than adjoint-based GD, attaining comparable or smaller reconstruction errors in far fewer iterations.

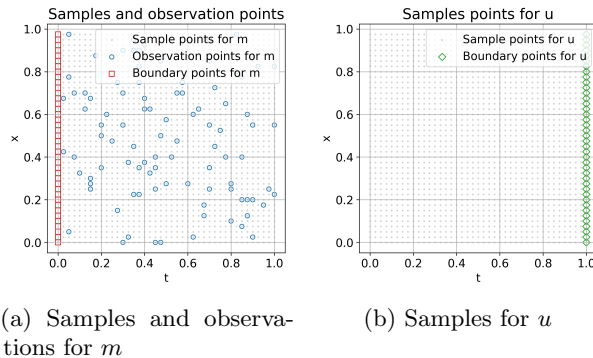


FIG. 8. The inverse problem of the time-dependent MFG in Section 4.3.1: samples for m and u & corresponding observation points.

4.3.2. Two-Dimensional Time-Dependent MFG Inverse Problem. In this example, we study the inverse problem for (4.5) on the flat torus $\mathbb{T}^2 \simeq [0, 1]^2$ with $T = 1$. We take $H(p) = \frac{1}{2}|p|^2$ and $\nu = 0.05$. The initial density is $m_0(x, y) = C \exp(-8[(x - 0.5)^2 + (y - 0.5)^2])$, where C is chosen so that $\int_{\mathbb{T}^2} m_0(x, y) dx dy = 1$, and the terminal condition is $u_T(x, y) = -m_0(x, y)$. We set $f(m) = m^3$ and $V(x, y) = \cos(2\pi x) \cos(2\pi y)$. With H , ν , f , and V fixed, we compute reference solutions (u^*, m^*) using the HRF. We then run GD and GN to reconstruct (u, m, V) , and report errors relative to (u^*, m^*, V^*) .

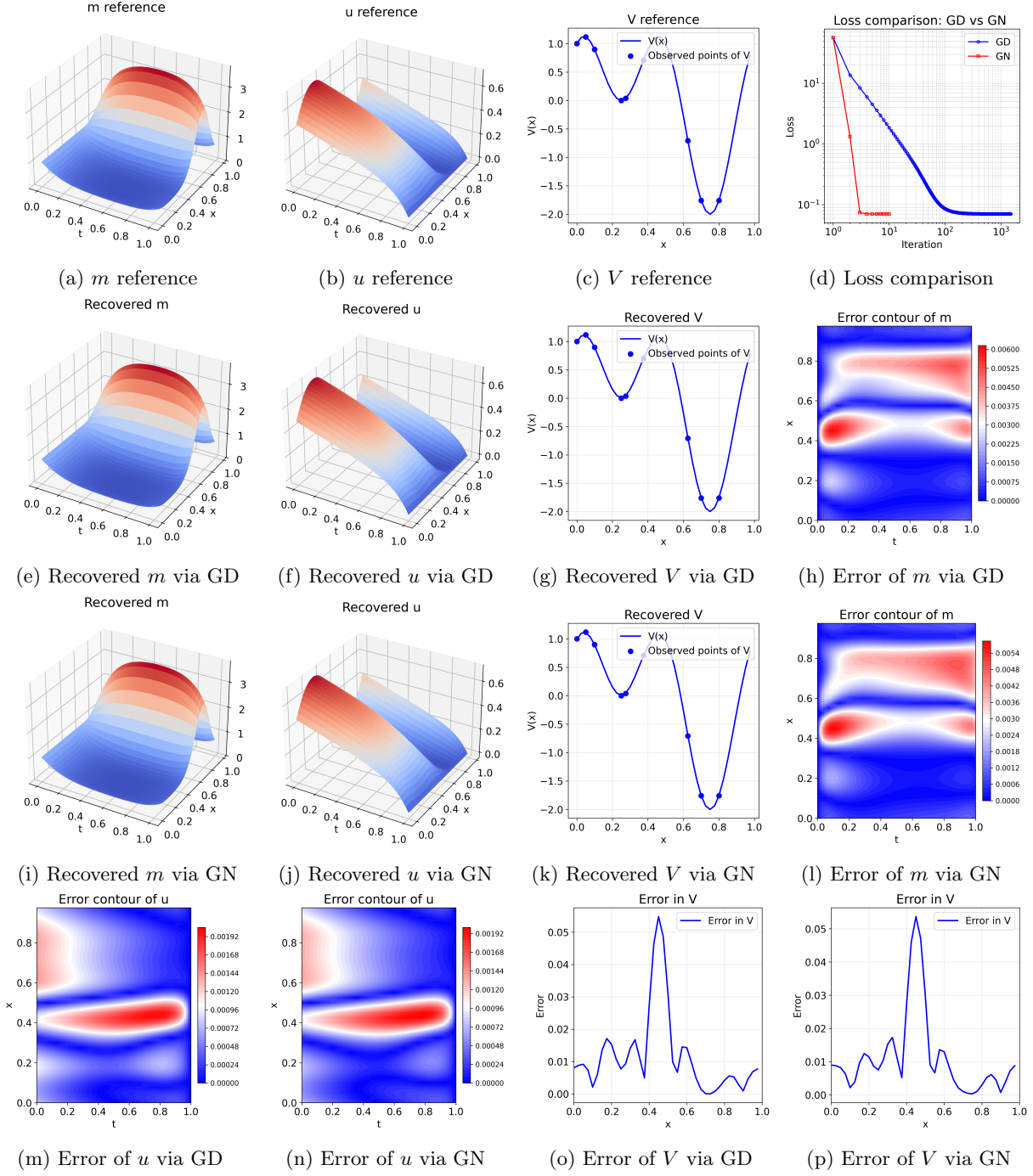


FIG. 9. Numerical results for the inverse problem of the time-dependent MFG in Section 4.3.1. (a), (b), (c) are references for m, u, V ; (d) log-log plot of the loss comparison for GD and GN across iterations; (e), (f), (g) recovered m, u, V via GD; (h), (m), (o) errors of m, u, V via GD; (i), (j), (k) recovered m, u, V via GN; (l), (n), (p) errors of m, u, V via GN.

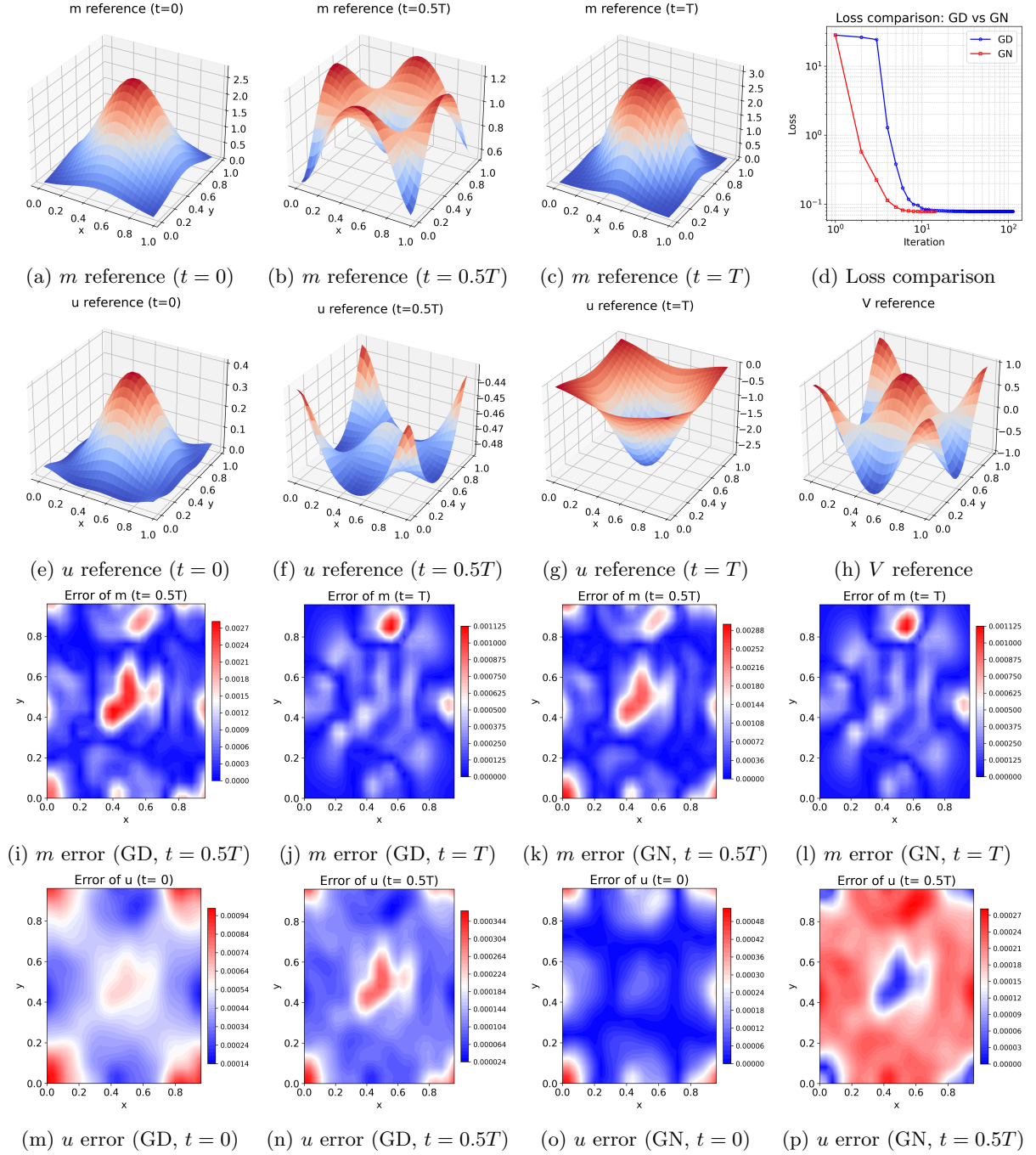


FIG. 10. Numerical results for the inverse problem of the 2D time-dependent MFG in Section 4.3.2. (a)-(c) reference m at $t = 0, 0.5T, T$; (d) log-log loss comparison of GD vs. GN; (e)-(g) reference u at $t = 0, 0.5T, T$; (h) time-independent reference V ; (i)-(j) error of m (GD) at $t = 0.5T, T$; (k)-(l) error of m (GN) at $t = 0.5T, T$; (m)-(n) error of u (GD) at $t = 0, 0.5T$; (o)-(p) error of u (GN) at $t = 0, 0.5T$.

Experimental Setup. We discretize \mathbb{T}^2 on a uniform 25×25 grid with spacing $h_x = h_y = \frac{1}{25}$, and discretize $[0, 1]$ with time step $h_t = \frac{1}{25}$, yielding $25^3 = 15625$ space-time grid points. On the temporal boundaries $t = 0$ and $t = T$, we use all $25^2 = 625$ spatial grid points at each time level. From the full space-time grid, we select 1250 observation samples of m , and we take 125 spatial observation locations for V . The regularization parameters are $\alpha = 0.04$, $\beta = 2$, and $\gamma = 2$. We perturb the observations with Gaussian noise $\mathcal{N}(0, \eta^2 I)$ with $\eta = 10^{-3}$. The initial guesses are $u \equiv 0$, $m \equiv 1$, and $V \equiv 0$.

Experimental Results. Figure 10 summarizes the two-dimensional, time-dependent MFG inverse problem. The reference density m at $t \in \{0, 0.5T, T\}$ is reported in Panels 10a–10c, the corresponding value function u is shown in Panels 10e–10g, and the reference spatial cost V is displayed in Panel 10h.

To assess reconstruction quality, Panel 10d plots the loss history. Pointwise absolute error contours for m are reported at $t = 0.5T$ and $t = T$ for GD (Panels 10i–10j) and GN (Panels 10k–10l). Likewise, pointwise error maps for u are shown at $t = 0$ and $t = 0.5T$ for GD (Panels 10m–10n) and GN (Panels 10o–10p).

The reconstruction of V is presented separately in Figure 11, which compares the recovered fields from GD and GN (Panels 11a and 11b) together with their pointwise absolute errors (Panels 11c and 11d). Overall, the loss history and the error fields across all reported time slices show that GN converges markedly faster than adjoint-based GD, attaining smaller errors in substantially fewer outer iterations.

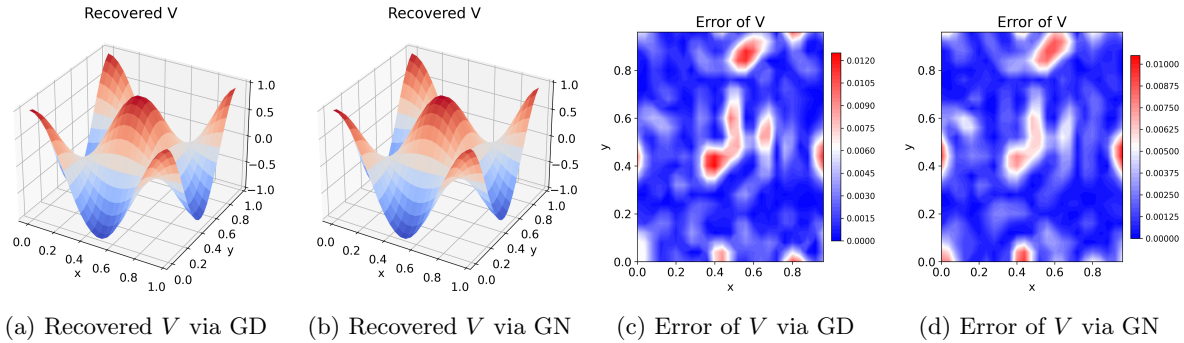


FIG. 11. Spatial cost V in 2D time-dependent MFG in Section 4.3.2. (a) recovered V via GD; (b) recovered V via GN; (c) error of V via GD; (d) error of V via GN.

5. CONCLUSION AND FUTURE WORK

In this paper, we develop a globally convergent method for time-dependent MFGs and a solver-agnostic framework for the MFG inverse problems. First, we develop a fully discrete HRF method for time-dependent MFG systems. We first discretize the MFG system and then construct the flow directly on the feasible manifold induced by the mixed end-point conditions and the slice-wise mass constraints. Under standard monotonicity and convexity structures, the resulting dynamics preserves positivity of the density and admits a global convergence guarantee in the discrete setting. This provides a forward solver whose feasibility properties are enforced by construction rather than by ad hoc corrections.

Second, we propose a solver-agnostic framework for inverse problems in stationary and time-dependent MFGs. We formulate the inverse task as an outer optimization over the unknown parameter while treating the discretized MFG equations as the defining constraints satisfied by the converged output of any inner forward solve. This viewpoint leads to an adjoint-based first-order method and a GN acceleration, both of which compute sensitivities by differentiating the discrete equilibrium constraints at the solved state, without differentiating through the inner solver iterations. We also note that, in the inverse setting, the forward model enters the outer objective only through the converged discrete state, as in (3.7). This suggests a modular viewpoint: the outer inversion procedure need only communicate with the inner forward solve through a prescribed interface for the discrete state and residual. In particular, different discretizations and inner solvers can be used internally, provided they return the state in the format required by the outer problem and supply a differentiable residual with respect to the state and the unknown parameters. Exploring this broader interface-based perspective is an interesting direction for future work.

Several directions remain to be explored. On the forward side, it is of interest to extend the discrete HRF construction beyond uniform periodic grids, for example, to non-periodic boundary conditions, nonuniform meshes, and more general couplings, while preserving the key monotonicity and feasibility structures. On the inverse side, further extensions include richer parameterizations of the unknown components. For instance, inspired by [61], the same framework could be used to recover the Hamiltonian and the coupling function jointly with the spatial cost, using only observations of agents' trajectories.

ACKNOWLEDGEMENT

HY acknowledges support in part by Hong Kong ECS Grant 21302521, Hong Kong RGC Grant 11311422, and Hong Kong RGC Grant 11303223. XY acknowledges support from the Air Force Office of Scientific Research through the MURI award FA9550-20-1-0358 (Machine Learning and Physics-Based Modeling and Simulation). XY also acknowledges support from the Air Force Office of Scientific Research under MURI award FOA-AFRL-AFOSR-2023-0004 (Mathematics of Digital Twins), the Department of Energy under award DE-SC0023163 (SEA-CROGS: Scalable, Efficient, and Accelerated Causal Reasoning Operators, Graphs and Spikes for Earth and Embedded Systems), the National Science Foundation under award 2425909 (Discovering the Law of Stress Transfer and Earthquake Dynamics in a Fault Network using a Computational Graph Discovery Approach), and the VBFF under ONR-N000142512035. JZ acknowledges support from the NUS Risk Management Institute research scholarship and the IoTeX Foundation Industry Grant A-8001180-00-00.

A. APPENDIX

We first recall the classical result from [2] that the discrete transport operator in the Fokker–Planck equation is the adjoint of the linearization of the discrete Hamiltonian.

Lemma A.1 (Discrete adjoint structure of the transport operator). *For any grid functions U , M , and V , one has*

$$\langle \mathcal{B}_h(U, M), V \rangle_h = \langle M \nabla_q g(\cdot, [D_h U]), [D_h V] \rangle_h, \quad (\text{A.1})$$

where $M \nabla_q g(\cdot, [D_h U])$ denotes componentwise multiplication. Equivalently, for fixed U , the operator $\mathcal{B}_h(U, \cdot)$ is the adjoint, with respect to $\langle \cdot, \cdot \rangle_h$, of the linearization of the map $V \mapsto g(\cdot, [D_h V])$ at U .

Proof. Fix U , M , and V . Write

$$Q_{i,j} := [D_h U]_{i,j} \in \mathbb{R}^4, \quad \nabla_q g_{i,j}(Q_{i,j}) = \left(\frac{\partial g_{i,j}}{\partial q_1}(Q_{i,j}), \frac{\partial g_{i,j}}{\partial q_2}(Q_{i,j}), \frac{\partial g_{i,j}}{\partial q_3}(Q_{i,j}), \frac{\partial g_{i,j}}{\partial q_4}(Q_{i,j}) \right).$$

By the definition of \mathcal{B}_h in (2.9),

$$\langle \mathcal{B}_h(U, M), V \rangle_h = \sum_{i,j} h^2 \mathcal{B}_h(U, M)_{i,j} V_{i,j}.$$

For arbitrary scalar grid functions $A = (A_{i,j})$ and $B = (B_{i,j})$ on the periodic grid, the one-sided difference operators satisfy the discrete summation-by-parts identities

$$\langle -D_1^- A, B \rangle_h = \langle A, D_1^+ B \rangle_h, \quad \langle -D_1^+ A, B \rangle_h = \langle A, D_1^- B \rangle_h.$$

Substituting the divergence form of $\mathcal{B}_h(U, M)$ and applying these identities yields

$$\begin{aligned} \langle \mathcal{B}_h(U, M), V \rangle_h &= \sum_{i,j} h^2 M_{i,j} \left(\frac{\partial g_{i,j}}{\partial q_1}(Q_{i,j}) (D_1^+ V)_{i,j} + \frac{\partial g_{i,j}}{\partial q_2}(Q_{i,j}) (D_1^- V)_{i,j} \right. \\ &\quad \left. + \frac{\partial g_{i,j}}{\partial q_3}(Q_{i,j}) (D_2^+ V)_{i,j} + \frac{\partial g_{i,j}}{\partial q_4}(Q_{i,j}) (D_2^- V)_{i,j} \right). \end{aligned}$$

By the definition of the stencil

$$[D_h V]_{i,j} = ((D_1^+ V)_{i,j}, (D_1^- V)_{i,j}, (D_2^+ V)_{i,j}, (D_2^- V)_{i,j}),$$

the right-hand side is exactly

$$\sum_{i,j} h^2 M_{i,j} \nabla_q g_{i,j}(Q_{i,j}) \cdot [D_h V]_{i,j},$$

which is

$$\langle M \nabla_q g(\cdot, [D_h U]), [D_h V] \rangle_h.$$

This proves (A.1).

The final statement follows immediately: for fixed M , the Fréchet derivative of the map

$$U \mapsto \langle M, g(\cdot, [D_h U]) \rangle_h$$

in the direction V is

$$\sum_{i,j} h^2 M_{i,j} \nabla_q g_{i,j}([D_h U]_{i,j}) \cdot [D_h V]_{i,j} = \langle \mathcal{B}_h(U, M), V \rangle_h.$$

Hence, for fixed U , the operator $\mathcal{B}_h(U, \cdot)$ is the adjoint, with respect to the discrete pairing, of the linearization of the discrete Hamiltonian block at U . \square

We next prove the monotonicity of the operator F_h defined in (2.14), as formalized in Proposition 2.1.

Proof of Proposition 2.1. Write

$$F_h(Y) = (r_1(Y), \dots, r_{N_T}(Y), s_1(Y), \dots, s_{N_T}(Y)),$$

where r_k, s_k are given by (2.12)–(2.13). By the definition of the space–time pairing,

$$\langle F_h(Y) - F_h(\tilde{Y}), Y - \tilde{Y} \rangle_{h,\Delta t} = \Delta t \sum_{k=1}^{N_T} \langle r_k(Y) - r_k(\tilde{Y}), M_k - \tilde{M}_k \rangle_h + \Delta t \sum_{k=1}^{N_T} \langle s_k(Y) - s_k(\tilde{Y}), U_{k-1} - \tilde{U}_{k-1} \rangle_h.$$

Step 1: time-derivative terms. Collecting the two discrete time-difference contributions and applying a telescoping sum yields the boundary term

$$\langle U_{N_T} - \tilde{U}_{N_T}, M_{N_T} - \tilde{M}_{N_T} \rangle_h - \langle U_0 - \tilde{U}_0, M_0 - \tilde{M}_0 \rangle_h.$$

Since $M_0 = \tilde{M}_0$ and $U_{N_T} = \tilde{U}_{N_T}$ are fixed endpoint samples, this term equals 0.

Step 2: diffusion terms. On the periodic grid \mathbb{T}_h^2 , the five-point Laplacian is self-adjoint with respect to $\langle \cdot, \cdot \rangle_h$, hence

$$\langle \Delta_h A, B \rangle_h = \langle A, \Delta_h B \rangle_h.$$

Therefore the diffusion contributions coming from r_k and s_k cancel:

$$\sum_{k=1}^{N_T} \nu \langle \Delta_h (U_{k-1} - \tilde{U}_{k-1}), M_k - \tilde{M}_k \rangle_h - \sum_{k=1}^{N_T} \nu \langle \Delta_h (M_k - \tilde{M}_k), U_{k-1} - \tilde{U}_{k-1} \rangle_h = 0.$$

Step 3: coupling terms. The coupling contribution equals

$$\Delta t \sum_{k=1}^{N_T} \langle f(M_k) - f(\tilde{M}_k), M_k - \tilde{M}_k \rangle_h.$$

By Assumption 2.2, each summand is nonnegative, and it is strictly positive whenever $M_k \neq \tilde{M}_k$. Hence

$$\Delta t \sum_{k=1}^{N_T} \langle f(M_k) - f(\tilde{M}_k), M_k - \tilde{M}_k \rangle_h \geq 0, \tag{A.2}$$

with equality only if $M_k = \tilde{M}_k$ for all k .

Step 4: Hamiltonian and transport terms. Fix $k \in \{1, \dots, N_T\}$ and set

$$\delta U := U_{k-1} - \tilde{U}_{k-1}, \quad \delta M := M_k - \tilde{M}_k.$$

Introduce the discrete Hamiltonian functional

$$\mathcal{G}_h(U) := g(\cdot, [D_h U]).$$

Using Lemma A.1, we obtain

$$\langle \mathcal{B}_h(U, M), V \rangle_h = \langle M \nabla_q g(\cdot, [D_h U]), [D_h V] \rangle_h \quad \text{for all } V. \tag{A.3}$$

Equivalently, for fixed M , the map

$$U \longmapsto \Phi_M(U) := \langle M, \mathcal{G}_h(U) \rangle_h$$

has Fréchet derivative

$$D\Phi_M(U)[V] = \langle \mathcal{B}_h(U, M), V \rangle_h.$$

Since each $q \mapsto g_{i,j}(q)$ is convex by Assumption 2.1, the functional Φ_M is convex for every nonnegative density M . Hence

$$\Phi_{\widetilde{M}_k}(U_{k-1}) - \Phi_{\widetilde{M}_k}(\widetilde{U}_{k-1}) - D\Phi_{\widetilde{M}_k}(\widetilde{U}_{k-1})[\delta U] \geq 0,$$

and

$$\Phi_{M_k}(\widetilde{U}_{k-1}) - \Phi_{M_k}(U_{k-1}) - D\Phi_{M_k}(U_{k-1})[-\delta U] \geq 0.$$

Expanding these two inequalities gives

$$\begin{aligned} & \langle \widetilde{M}_k, g(\cdot, [D_h U_{k-1}]) - g(\cdot, [D_h \widetilde{U}_{k-1}]) \rangle_h - \langle \mathcal{B}_h(\widetilde{U}_{k-1}, \widetilde{M}_k), \delta U \rangle_h \geq 0, \\ & - \langle M_k, g(\cdot, [D_h U_{k-1}]) - g(\cdot, [D_h \widetilde{U}_{k-1}]) \rangle_h + \langle \mathcal{B}_h(U_{k-1}, M_k), \delta U \rangle_h \geq 0. \end{aligned}$$

Adding them yields

$$\langle g(\cdot, [D_h \widetilde{U}_{k-1}] - g(\cdot, [D_h U_{k-1}]), \delta M \rangle_h + \langle \mathcal{B}_h(U_{k-1}, M_k) - \mathcal{B}_h(\widetilde{U}_{k-1}, \widetilde{M}_k), \delta U \rangle_h \geq 0. \quad (\text{A.4})$$

If $q \mapsto g_{i,j}(q)$ is strictly convex, then the inequality in (A.4) is strict whenever

$$[D_h U_{k-1}] \neq [D_h \widetilde{U}_{k-1}].$$

Step 5: conclusion. Adding Steps 1–4 yields

$$\langle F_h(Y) - F_h(\widetilde{Y}), Y - \widetilde{Y} \rangle_{h, \Delta t} \geq 0.$$

Moreover, if $Y \neq \widetilde{Y}$, then either $M_k \neq \widetilde{M}_k$ for some k , in which case the coupling term in Step 3 is strictly positive, or $U_{k-1} \neq \widetilde{U}_{k-1}$ for some k , in which case the Hamiltonian–transport term in Step 4 is strictly positive. Therefore

$$\langle F_h(Y) - F_h(\widetilde{Y}), Y - \widetilde{Y} \rangle_{h, \Delta t} > 0 \quad \text{for all } Y \neq \widetilde{Y},$$

which proves (2.15). \square

Next, we establish the explicit formulas for the HRF method as described in Proposition 2.2.

Proof of Proposition 2.2. Fix a feasible state Y with $M_k \in \mathcal{M}_{+,h}$ for $k = 1, \dots, N_T$ and consider the minimization problem (2.17). Since $M_k > 0$ componentwise, the operator $\mathcal{H}_h(Y)$ is positive definite on each block, hence the quadratic map $\Xi \mapsto \frac{1}{2} g_{Y,h}(\Xi, \Xi)$ is strictly convex on \mathcal{Y}_h . Therefore, the objective in (2.17) is strictly convex, and minimizing it over the affine subspace $\mathcal{T}_{Y,h}$ admits a unique minimizer.

Introduce Lagrange multipliers $\lambda_k \in \mathbb{R}$ for the constraints $\langle \Xi_{M_k}, \mathbf{1} \rangle_h = 0$ and define the Lagrangian

$$\mathcal{L}(\Xi, \lambda) := \frac{1}{2} g_{Y,h}(\Xi, \Xi) + \langle F_h(Y), \Xi \rangle_{h, \Delta t} + \Delta t \sum_{k=1}^{N_T} \lambda_k \langle \Xi_{M_k}, \mathbf{1} \rangle_h.$$

We recall that $g_{Y,h}(\Xi, \Psi) = \langle \mathcal{H}_h(Y) \Xi, \Psi \rangle_{h, \Delta t}$. For the unconstrained U -blocks, fix $k \in \{1, \dots, N_T\}$ and take an arbitrary variation $\delta \Xi_{U_{k-1}} \in \mathbb{R}^{N_x}$, keeping all other blocks fixed. Then

$$0 = \delta_{\Xi_{U_{k-1}}} \mathcal{L}(\Xi, \lambda) [\delta \Xi_{U_{k-1}}] = \Delta t \langle \Xi_{U_{k-1}} + s_k(Y), \delta \Xi_{U_{k-1}} \rangle_h.$$

Since $\delta \Xi_{U_{k-1}}$ is arbitrary and $\Delta t > 0$, we conclude that

$$\Xi_{U_{k-1}} = -s_k(Y). \quad (\text{A.5})$$

For the constrained density blocks, fix $k \in \{1, \dots, N_T\}$ and take an arbitrary variation $\delta \Xi_{M_k} \in \mathbb{R}^{N_x}$. Using that the M_k -block of $\mathcal{H}_h(Y)$ equals $\text{diag}(1/M_k)$, we obtain

$$0 = \delta_{\Xi_{M_k}} \mathcal{L}(\Xi, \lambda) [\delta \Xi_{M_k}] = \Delta t \left\langle \frac{\Xi_{M_k}}{M_k} + r_k(Y) + \lambda_k \mathbf{1}, \delta \Xi_{M_k} \right\rangle_h.$$

Again $\delta\Xi_{M_k}$ is arbitrary, hence

$$\frac{\Xi_{M_k}}{M_k} + r_k(Y) + \lambda_k \mathbf{1} = 0, \quad \text{or equivalently} \quad \Xi_{M_k} = -M_k \odot (r_k(Y) + \lambda_k \mathbf{1}). \quad (\text{A.6})$$

Imposing the constraint $\langle \Xi_{M_k}, \mathbf{1} \rangle_h = 0$ and using $\langle M_k \odot a, \mathbf{1} \rangle_h = \langle M_k, a \rangle_h$ gives

$$0 = \langle \Xi_{M_k}, \mathbf{1} \rangle_h = -\langle M_k, r_k(Y) \rangle_h - \lambda_k \langle M_k, \mathbf{1} \rangle_h,$$

so

$$\lambda_k = -\frac{\langle M_k, r_k(Y) \rangle_h}{\langle M_k, \mathbf{1} \rangle_h} = -\bar{r}_k(Y).$$

Substituting this into (A.6) yields

$$\Xi_{M_k} = -M_k \odot (r_k(Y) - \bar{r}_k(Y) \mathbf{1}), \quad k = 1, \dots, N_T.$$

Finally, identifying the minimizer Ξ in (2.17) with $\dot{Y}(s)$ yields (2.19), which completes the proof. \square

Then, we establish the existence of the HRF dynamics and show that it preserves positivity and mass.

Proof of Proposition 2.3. Assumption 2.3 implies that $Y \mapsto (r_1(Y), \dots, r_{N_T}(Y), s_1(Y), \dots, s_{N_T}(Y))$ is locally Lipschitz on the feasible interior. Since (2.19) is obtained from these blocks by smooth algebraic operations on that interior, the vector field in (2.19) is locally Lipschitz there. Therefore, by the Picard–Lindelöf theorem, there exists a unique solution $Y(\cdot)$ on some interval $[0, S_{\max})$ with $S_{\max} > 0$.

Along the solution, the mass identity follows directly from (2.19). Indeed, using $\langle a \odot b, \mathbf{1} \rangle_h = \langle a, b \rangle_h$ and the definition (2.18), for each k and all $s \in [0, S_{\max})$,

$$\frac{d}{ds} \langle M_k(s), \mathbf{1} \rangle_h = -\langle M_k(s), r_k(Y(s)) - \bar{r}_k(Y(s)) \mathbf{1} \rangle_h = -\langle M_k(s), r_k(Y(s)) \rangle_h + \bar{r}_k(Y(s)) \langle M_k(s), \mathbf{1} \rangle_h = 0.$$

Hence

$$\langle M_k(s), \mathbf{1} \rangle_h = \langle M_k(0), \mathbf{1} \rangle_h = 1 \quad \text{for all } s \in [0, S_{\max}).$$

Positivity follows from the multiplicative structure of the density equation. Fix k and a component index α . Writing

$$B_k(Y) := r_k(Y) - \bar{r}_k(Y) \mathbf{1},$$

the k th density block satisfies

$$\dot{M}_k = -M_k \odot B_k(Y).$$

Thus,

$$\frac{d}{ds} \log(M_k(s))_\alpha = -(B_k(Y(s)))_\alpha,$$

and

$$(M_k(s))_\alpha = (M_k(0))_\alpha \exp\left(-\int_0^s (B_k(Y(\sigma)))_\alpha d\sigma\right) > 0 \quad \text{for all } s \in [0, S_{\max}).$$

Hence, $M_k(s)$ remains strictly positive componentwise on $[0, S_{\max})$, and together with the mass constraint we have

$$M_k(s) \in \mathcal{M}_{++h} \quad \text{for all } s \in [0, S_{\max}).$$

It remains to show that $S_{\max} = +\infty$. Let \mathcal{E} be the discrete entropy (2.16). We interpret $\nabla \mathcal{E}$ as the gradient with respect to the space-time pairing $\langle \cdot, \cdot \rangle_{h, \Delta t}$, i.e. $D\mathcal{E}(Y)[\Xi] = \langle \nabla \mathcal{E}(Y), \Xi \rangle_{h, \Delta t}$, and define the associated Bregman divergence

$$D_{\mathcal{E}}(Y^*, Y) := \mathcal{E}(Y^*) - \mathcal{E}(Y) - \langle \nabla \mathcal{E}(Y), Y^* - Y \rangle_{h, \Delta t}.$$

Fix $s \in [0, S_{\max})$. Since both $Y(s)$ and Y^* belong to \mathcal{M}_h , their difference $Y^* - Y(s)$ lies in the tangent space $T_{Y(s)} \mathcal{M}_h$. Therefore, we may use $\Xi = Y^* - Y(s)$ as a test direction in the variational characterization (2.17), which gives

$$g_{Y(s), \mathcal{E}}(\dot{Y}(s), Y^* - Y(s)) = -\langle F_h(Y(s)), Y^* - Y(s) \rangle_{h, \Delta t}.$$

On the other hand, by the chain rule and the definition of $D_{\mathcal{E}}$,

$$\frac{d}{ds} D_{\mathcal{E}}(Y^*, Y(s)) = -\langle \nabla^2 \mathcal{E}(Y(s)) \dot{Y}(s), Y^* - Y(s) \rangle_{h, \Delta t} = -g_{Y(s), \mathcal{E}}(\dot{Y}(s), Y^* - Y(s)).$$

Combining the two identities yields

$$\frac{d}{ds} D_{\mathcal{E}}(Y^*, Y(s)) = \langle F_h(Y(s)), Y^* - Y(s) \rangle_{h, \Delta t}.$$

Since $F_h(Y^*) = 0$, we obtain

$$\frac{d}{ds} D_{\mathcal{E}}(Y^*, Y(s)) = -\langle F_h(Y(s)) - F_h(Y^*), Y(s) - Y^* \rangle_{h, \Delta t}.$$

By Proposition 2.1, the operator F_h is monotone on \mathcal{M}_h , hence

$$\frac{d}{ds} D_{\mathcal{E}}(Y^*, Y(s)) \leq 0.$$

Therefore $s \mapsto D_{\mathcal{E}}(Y^*, Y(s))$ is nonincreasing on $[0, S_{\max}]$.

This Lyapunov bound prevents the solution from approaching the boundary of the feasible interior in finite flow time. Indeed, the quadratic part of \mathcal{E} implies a uniform bound on the U -blocks in $\|\cdot\|_{h, \Delta t}$ on any interval $[0, S]$ with $S < S_{\max}$. For the density blocks, note that $D_{\mathcal{E}}(Y^*, Y)$ contains the discrete relative-entropy terms

$$\Delta t \sum_{k=1}^{N_T} \sum_{\alpha} h^2 \left[(M_k^*)_{\alpha} \log \frac{(M_k^*)_{\alpha}}{(M_k)_{\alpha}} - ((M_k^*)_{\alpha} - (M_k)_{\alpha}) \right].$$

Since $M_k^* > 0$ componentwise, if some component $(M_k)_{\alpha}$ were to tend to 0, the corresponding term $(M_k^*)_{\alpha} \log \frac{(M_k^*)_{\alpha}}{(M_k)_{\alpha}}$ would diverge to $+\infty$, contradicting boundedness of $D_{\mathcal{E}}(Y^*, Y(s)) \leq D_{\mathcal{E}}(Y^*, Y^0)$. Consequently, for each finite $S < S_{\max}$ there exists $c_S > 0$ such that $(M_k(s))_{\alpha} \geq c_S$ for all $s \in [0, S]$, all k , and all components. Together with mass preservation, which yields the pointwise upper bound $(M_k(s))_{\alpha} \leq \frac{1}{h^2}$, this shows that $Y(s)$ remains in a compact subset of the feasible interior on every finite time interval.

Because the vector field in (2.19) is locally Lipschitz on the feasible interior, the standard continuation criterion for ODEs in finite dimension implies that the maximal solution cannot terminate at a finite time while staying in a compact subset of the domain. Hence $S_{\max} = +\infty$. The positivity and mass identities established above, therefore, hold for all $s \geq 0$. \square

The following proof establishes global convergence of the HRF method and shows that convergence does not require a carefully chosen initialization.

Proof of Theorem 2.4. By Proposition 2.3, the solution $Y(s)$ of (2.19) exists for all $s \geq 0$ and remains feasible. In particular, for each $k = 1, \dots, N_T$, one has $\langle M_k(s), \mathbf{1} \rangle_h = 1$ and $M_k(s) \in \mathcal{M}_{+,+,h}$ for all $s \geq 0$. According to the proof of Proposition 2.3, $D_{\mathcal{E}}(Y^*, Y(s))$ is nonincreasing, and the trajectory $\{Y(s) : s \geq 0\}$ remains in a compact subset K of the feasible interior.

Now define

$$\Phi(s) := \langle F_h(Y(s)) - F_h(Y^*), Y(s) - Y^* \rangle_{h, \Delta t} \geq 0.$$

We have $\frac{d}{ds} D_{\mathcal{E}}(Y^*, Y(s)) = -\Phi(s)$, and therefore

$$\int_0^{\infty} \Phi(s) ds = D_{\mathcal{E}}(Y^*, Y(0)) - \lim_{s \rightarrow \infty} D_{\mathcal{E}}(Y^*, Y(s)) < \infty.$$

Since $Y(s)$ remains in the compact set K and the vector field in (2.19) is continuous on K , the derivative $\dot{Y}(s)$ is bounded on $[0, \infty)$. Hence Y is uniformly continuous on $[0, \infty)$. Moreover, the map $Y \mapsto \langle F_h(Y) - F_h(Y^*), Y - Y^* \rangle_{h, \Delta t}$ is continuous on K , hence uniformly continuous there. It follows that Φ is uniformly continuous on $[0, \infty)$. By Barbalat's lemma [34], $\Phi(s) \rightarrow 0$ as $s \rightarrow \infty$.

Let $s_n \rightarrow \infty$ be arbitrary. Since the trajectory is precompact, after passing to a subsequence, we may assume that $Y(s_n) \rightarrow \bar{Y} \in \mathcal{M}_h$. By continuity of Φ ,

$$0 = \lim_{n \rightarrow \infty} \Phi(s_n) = \langle F_h(\bar{Y}) - F_h(Y^*), \bar{Y} - Y^* \rangle_{h, \Delta t}.$$

By the strict monotonicity of F_h on \mathcal{M}_h , this implies $\bar{Y} = Y^*$. Hence every accumulation point of $Y(s)$ is equal to Y^* , and therefore $Y(s) \rightarrow Y^*$ as $s \rightarrow \infty$.

Finally, by continuity of F_h , we also obtain $F_h(Y(s)) \rightarrow F_h(Y^*) = 0$ as $s \rightarrow \infty$. \square

Now, we are ready to compute the gradient of the inverse objective with respect to the unknown coefficients.

Proof of Proposition 3.2. Fix $\theta \in \Theta$ and an arbitrary direction $\delta\theta \in \mathbb{R}^p$. Set

$$\delta z := \frac{\partial z^*(\theta)}{\partial \theta} \delta\theta \in \mathbb{R}^n.$$

Differentiating the reduced objective (3.7) gives

$$d\mathcal{J}(\theta)[\delta\theta] = \beta (Wz^*(\theta) - z^\circ)^\top W \delta z + \gamma (G\theta - \theta^\circ)^\top G \delta\theta + \alpha (J\theta)^\top J \delta\theta. \quad (\text{A.7})$$

The dependence of $d\mathcal{J}$ on $\delta\theta$ is implicit through δz .

Next, differentiate the equilibrium constraints (3.6). From $F(z^*(\theta), \theta) = 0$ we obtain

$$\frac{\partial F}{\partial z}(z^*(\theta), \theta) \delta z + \frac{\partial F}{\partial \theta}(z^*(\theta), \theta) \delta\theta = 0. \quad (\text{A.8})$$

From the linear constraints $Az^*(\theta) = \mathbf{b}$ we obtain

$$A \delta z = 0. \quad (\text{A.9})$$

When $q = 0$ (constraints eliminated), (A.9) is absent, and the argument below holds with η omitted.

Introduce multipliers $\psi \in \mathbb{R}^n$ and $\eta \in \mathbb{R}^q$, and add to (A.7) the identities obtained by pairing (A.8) with ψ and (A.9) with η :

$$0 = \psi^\top \left(\frac{\partial F}{\partial z}(z^*(\theta), \theta) \delta z + \frac{\partial F}{\partial \theta}(z^*(\theta), \theta) \delta\theta \right), \quad 0 = \eta^\top (A \delta z).$$

Rearranging yields

$$\begin{aligned} d\mathcal{J}(\theta)[\delta\theta] &= \left[\beta W^\top (Wz^*(\theta) - z^\circ) + \frac{\partial F}{\partial z}(z^*(\theta), \theta)^\top \psi + A^\top \eta \right]^\top \delta z \\ &\quad + \left[\frac{\partial F}{\partial \theta}(z^*(\theta), \theta)^\top \psi + \gamma G^\top (G\theta - \theta^\circ) + \alpha J^\top J \theta \right]^\top \delta\theta. \end{aligned} \quad (\text{A.10})$$

We now choose (ψ, η) so that the coefficient of δz vanishes, namely

$$\frac{\partial F}{\partial z}(z^*(\theta), \theta)^\top \psi + A^\top \eta = -\beta W^\top (Wz^*(\theta) - z^\circ). \quad (\text{A.11})$$

To ensure compatibility with the linear constraint (A.9) (and to fix the component of ψ in $\text{range}(A^\top)$), we additionally impose

$$A \psi = 0. \quad (\text{A.12})$$

Together, (A.11)–(A.12) are exactly (3.8). With this choice, the δz term in (A.10) cancels and we obtain

$$d\mathcal{J}(\theta)[\delta\theta] = \left[\frac{\partial F}{\partial \theta}(z^*(\theta), \theta)^\top \psi + \gamma G^\top (G\theta - \theta^\circ) + \alpha J^\top J \theta \right]^\top \delta\theta.$$

Since $\delta\theta$ is arbitrary, this identifies the gradient as (3.9). \square

Finally, we derive the update formulas for the GN method.

Proof of Proposition 3.3. The GN method is applied to the least-squares objective

$$\mathcal{J}(\theta) = \frac{1}{2} \|r(\theta)\|_2^2,$$

and is based on the first-order approximation

$$r(\theta + p) \approx r(\theta) + J_r(\theta)p.$$

Therefore, to determine the Jacobian action $J_r(\theta)p$, we differentiate the residual (3.10) with respect to the parameter perturbation p .

The second and third residual blocks depend explicitly on θ , so their first-order variations are simply $\sqrt{\gamma} Gp$ and $\sqrt{\alpha} Jp$. The first residual block depends on θ through the equilibrium state $z^*(\theta)$. Let δz_p denote the corresponding first-order variation, defined by

$$z^*(\theta + \varepsilon p) = z^*(\theta) + \varepsilon \delta z_p + o(\varepsilon) \quad \text{as } \varepsilon \rightarrow 0.$$

Since $z^*(\theta)$ satisfies the equilibrium constraints

$$F(z^*(\theta), \theta) = 0, \quad Az^*(\theta) = \mathbf{b},$$

differentiating these relations with respect to ε at $\varepsilon = 0$ yields

$$\frac{\partial F}{\partial z}(z^*(\theta), \theta) \delta z_p + \frac{\partial F}{\partial \theta}(z^*(\theta), \theta) p = 0, \quad A \delta z_p = 0,$$

which is exactly (3.12). It follows that the first residual block has variation $\sqrt{\beta} W \delta z_p$. Collecting the three blocks gives

$$J_r(\theta)p = \begin{bmatrix} \sqrt{\beta} W \delta z_p \\ \sqrt{\gamma} G p \\ \sqrt{\alpha} J p \end{bmatrix}.$$

It remains to characterize the GN step. By definition, p minimizes the linearized least-squares functional

$$\frac{1}{2} \|r(\theta) + J_r(\theta)p\|_2^2.$$

Differentiating this quadratic functional with respect to p and setting the result equal to zero gives

$$J_r(\theta)^\top (r(\theta) + J_r(\theta)p) = 0.$$

Rearranging yields (3.13). □

REFERENCES

- [1] Y. Achdou, F. Camilli, and I. Capuzzo-Dolcetta. Mean field games: Convergence of a finite difference method. *SIAM Journal on Numerical Analysis*, 51(5):2585–2612, 2013.
- [2] Y. Achdou and I. Capuzzo-Dolcetta. Mean field games: Numerical methods. *SIAM Journal on Numerical Analysis*, 48(3):1136–1162, 2010.
- [3] Y. Achdou and V. Perez. Iterative strategies for solving linearized discrete mean field games systems. *Networks and Heterogeneous Media*, 7(2):197, 2012.
- [4] A. Agrawal, B. Amos, S. Barratt, S. Boyd, S. Diamond, and J. Z. Kolter. Differentiable convex optimization layers. *Advances in Neural Information Processing Systems*, 32, 2019.
- [5] N. Almulla, R. Ferreira, and D. A. Gomes. Two numerical approaches to stationary mean-field games. *Dynamic Games and Applications*, 7(4):657–682, 2017.
- [6] B. Amos and J. Z. Kolter. Optnet: Differentiable optimization as a layer in neural networks. In *International Conference on Machine Learning*, pages 136–145. PMLR, 2017.
- [7] T. Bakaryan, C. Aoun, R. D. L. Ribeiro, N. Hovakimyan, and D. A. Gomes. Hessian Riemannian flow for multi-population Wardrop equilibrium. *arXiv preprint arXiv:2504.16028*, 2025.
- [8] M. Blondel, Q. Berthet, M. Cuturi, R. Frostig, S. Hoyer, F. Llinares-López, F. Pedregosa, and J.-P. Vert. Efficient and modular implicit differentiation. *Advances in Neural Information Processing Systems*, 35:5230–5242, 2022.
- [9] L. M. Briceno-Arias, D. Kalise, Z. Kobeissi, M. Laurière, A. M. González, and F. Silva. On the implementation of a primal-dual algorithm for second order time-dependent mean field games with local couplings. *ESAIM: Proceedings and Surveys*, 65:330–348, 2019.
- [10] L. M. Briceno-Arias, D. Kalise, and F. Silva. Proximal methods for stationary mean field games with local couplings. *SIAM Journal on Control and Optimization*, 56(2):801–836, 2018.
- [11] L. M. Briceno-Arias, F. J. Silva, and X. Yang. Forward-backward algorithm for functions with locally Lipschitz gradient: applications to mean field games. *Set-Valued and Variational Analysis*, 32(2):16, 2024.
- [12] S. Cacace, F. Camilli, and A. Goffi. A policy iteration method for mean field games. *ESAIM: Control, Optimisation and Calculus of Variations*, 27:85, 2021.
- [13] P. Cardaliaguet. Notes on mean field games. Technical report, Technical report Technical report, 2010.
- [14] P. Cardaliaguet. Long time average of first order mean field games and weak KAM theory. *Dynamic Games and Applications*, 3(4):473–488, 2013.
- [15] P. Cardaliaguet, J.-M. Lasry, P.-L. Lions, and A. Porretta. Long time average of mean field games. *Networks & Heterogeneous Media*, 7(2), 2012.
- [16] P. Cardaliaguet and C.-A. Lehalle. Mean field game of controls and an application to trade crowding. *Mathematics and Financial Economics*, 12(3):335–363, 2018.
- [17] P. Cardaliaguet and A. Porretta. An introduction to mean field game theory. In *Mean Field Games: Cetraro, Italy 2019*, pages 1–158. Springer, 2021.
- [18] E. Carlini and F. J. Silva. A semi-Lagrangian scheme for a degenerate second order mean field game system. *Discrete and Continuous Dynamical Systems*, 35(9):4269–4292, 2015.
- [19] E. Carlini, F. J. Silva, and A. Zorkot. A Lagrange–Galerkin scheme for first order mean field game systems. *SIAM Journal on Numerical Analysis*, 62(1):167–198, 2024.
- [20] R. Carmona and M. Laurière. Convergence analysis of machine learning algorithms for the numerical solution of mean field control and games I: The ergodic case. *SIAM Journal on Numerical Analysis*, 59(3):1455–1485, 2021.
- [21] R. Carmona and M. Laurière. Convergence analysis of machine learning algorithms for the numerical solution of mean field control and games: II—the finite horizon case. *The Annals of Applied Probability*, 32(6):4065–4105, 2022.

- [22] Y. Chen, B. Hosseini, H. Owhadi, and A. M. Stuart. Solving and learning nonlinear PDEs with Gaussian processes. *Journal of Computational Physics*, 447:110668, 2021.
- [23] L. Ding, W. Li, S. Osher, and W. Yin. A mean field game inverse problem. *Journal of Scientific Computing*, 92(1):7, 2022.
- [24] D. A. Gomes, E. A. Pimentel, and V. Voskanyan. *Regularity theory for mean-field game systems*. Springer, 2016.
- [25] D. A. Gomes and J. Saúde. Mean field games models—a brief survey. *Dynamic Games and Applications*, 4(2):110–154, 2014.
- [26] D. A. Gomes and J. Saúde. Monotone numerical methods for finite-state mean-field games. *arXiv preprint arXiv:1705.00174*, 2017.
- [27] D. A. Gomes and J. Saúde. Numerical methods for finite-state mean-field games satisfying a monotonicity condition. *Applied Mathematics & Optimization*, 83(1):51–82, 2021.
- [28] D. A. Gomes and X. Yang. The Hessian Riemannian flow and Newton’s method for effective Hamiltonians and Mather measures. *ESAIM: Mathematical Modelling and Numerical Analysis*, 54(6):1883–1915, 2020.
- [29] J. Guo, C. Mou, X. Yang, and C. Zhou. Decoding mean field games from population and environment observations by Gaussian processes. *Journal of Computational Physics*, 508:112978, 2024.
- [30] H. Huang, J. Yu, T. Chen, and R. Lai. Joint inference of trajectory and obstacle in mean-field games via bilevel optimization. *arXiv preprint arXiv:2507.19344*, 2025.
- [31] M. Huang, P. E. Caines, and R. P. Malhamé. Large-population cost-coupled LQG problems with nonuniform agents: Individual-mass behavior and decentralized ε -Nash equilibria. *IEEE Transactions on Automatic Control*, 52(9):1560–1571, 2007.
- [32] M. Huang, R. P. Malhamé, and P. E. Caines. Large population stochastic dynamic games: closed-loop McKean-Vlasov systems and the Nash certainty equivalence principle. *Communications in Information and Systems*, 6(3):221–252, 2006.
- [33] O. Imanuvilov, H. Liu, and M. Yamamoto. Lipschitz stability for determination of states and inverse source problem for the mean field game equations. *Inverse Problems and Imaging*, 18(4):824–859, 2024.
- [34] H. K. Khalil and J. W. Grizzle. *Nonlinear systems*, volume 3. Prentice hall Upper Saddle River, NJ, 2002.
- [35] M. V. Klibanov, J. Li, and H. Liu. Hölder stability and uniqueness for the mean field games system via Carleman estimates. *Studies in Applied Mathematics*, 151(4):1447–1470, 2023.
- [36] M. V. Klibanov, J. Li, and Z. Yang. Convexification for a coefficient inverse problem for a system of two coupled nonlinear parabolic equations. *Computers & Mathematics with Applications*, 179:41–58, 2025.
- [37] A. Lachapelle, J.-M. Lasry, C.-A. Lehalle, and P.-L. Lions. Efficiency of the price formation process in presence of high frequency participants: a mean field game analysis. *Mathematics and Financial Economics*, 10(3):223–262, 2016.
- [38] J.-M. Lasry and P.-L. Lions. Jeux à champ moyen. i—le cas stationnaire. *Comptes Rendus Mathématique*, 343(9):619–625, 2006.
- [39] J.-M. Lasry and P.-L. Lions. Jeux à champ moyen. ii—horizon fini et contrôle optimal. *Comptes Rendus. Mathématique*, 343(10):679–684, 2006.
- [40] J.-M. Lasry and P.-L. Lions. Mean field games. *Japanese Journal of Mathematics*, 2(1):229–260, 2007.
- [41] M. Laurière, J. Song, and Q. Tang. Policy iteration method for time-dependent mean field games systems with non-separable Hamiltonians. *Applied Mathematics & Optimization*, 87(2):17, 2023.
- [42] A. T. Lin, S. W. Fung, W. Li, L. Nurbekyan, and S. J. Osher. Alternating the population and control neural networks to solve high-dimensional stochastic mean-field games. *Proceedings of the National Academy of Sciences*, 118(31):e2024713118, 2021.
- [43] H. Liu, C. Mou, and S. Zhang. Inverse problems for mean field games. *Inverse Problems*, 39(8):085003, 2023.
- [44] S. Liu, M. Jacobs, W. Li, L. Nurbekyan, and S. J. Osher. Computational methods for first-order nonlocal mean field games with applications. *SIAM Journal on Numerical Analysis*, 59(5):2639–2668, 2021.
- [45] S. Liu and L. Nurbekyan. Splitting methods for a class of non-potential mean field games. *Journal of Dynamics and Games*, 8(4):467–486, 2021.
- [46] R. Meng and X. Yang. Sparse Gaussian processes for solving nonlinear PDEs. *Journal of Computational Physics*, 490:112340, 2023.
- [47] C. Mou, X. Yang, and C. Zhou. Numerical methods for mean field games based on Gaussian processes and Fourier features. *Journal of Computational Physics*, 460:111188, 2022.
- [48] L. Nurbekyan and J. Saúde. Fourier approximation methods for first-order nonlocal mean-field games. *Portugaliae Mathematica*, 75(3):367–396, 2019.
- [49] Y. A. Osborne and I. Smears. Finite element approximation of time-dependent mean field games with nondifferentiable hamiltonians. *Numerische Mathematik*, 157(1):165–211, 2025.
- [50] H. Owhadi and C. Scovel. *Operator-Adapted Wavelets, Fast Solvers, and Numerical Homogenization: From a Game Theoretic Approach to Numerical Approximation and Algorithm Design*, volume 35. Cambridge University Press, 2019.
- [51] K. Ren, N. Soedjak, and S. Tong. A policy iteration method for inverse mean field games. *arXiv preprint arXiv:2409.06184*, 2024.
- [52] K. Ren, N. Soedjak, K. Wang, and H. Zhai. Reconstructing a state-independent cost function in a mean-field game model. *Inverse Problems*, 40(10):105010, 2024.
- [53] L. Ruthotto, S. J. Osher, W. Li, L. Nurbekyan, and S. W. Fung. A machine learning framework for solving high-dimensional mean field game and mean field control problems. *Proceedings of the National Academy of Sciences*, 117(17):9183–9193, 2020.
- [54] H. Wendland. *Scattered data approximation*, volume 17. Cambridge University Press, 2004.

- [55] L. Yang, S. Liu, T. Meng, and S. J. Osher. In-context operator learning with data prompts for differential equation problems. *Proceedings of the National Academy of Sciences*, 120(39):e2310142120, 2023.
- [56] L. Yang, X. Sun, B. Hamzi, H. Owhadi, and N. Xie. Learning dynamical systems from data: A simple cross-validation perspective, part V: Sparse kernel flows for 132 chaotic dynamical systems. *Physica D: Nonlinear Phenomena*, 460:134070, 2024.
- [57] X. Yang and H. Owhadi. A mini-batch method for solving nonlinear PDEs with Gaussian processes. *arXiv preprint arXiv:2306.00307*, 2023.
- [58] X. Yang and J. Zhang. Gaussian process policy iteration with additive Schwarz acceleration for forward and inverse HJB and mean field game problems. *arXiv preprint arXiv:2505.00909*, 2025.
- [59] J. Yu, J. Liu, and H. Zhao. Equilibrium correction iteration for a class of mean-field game inverse problems. *Inverse Problems*, 41(12):125009, 2025.
- [60] J. Yu, Q. Xiao, T. Chen, and R. Lai. A bilevel optimization method for inverse mean-field games. *Inverse Problems*, 40(10):105016, 2024.
- [61] J. Zhang, X. Yang, C. Mou, and C. Zhou. Learning surrogate potential mean field games via Gaussian processes: A data-driven approach to ill-posed inverse problems. *Journal of Computational Physics*, 543:114412, 2025.